MSc (Petroleum Engineering)

Project Report 2017

Juan Tomasini

Assessment of the Potential for Gas Production from Marine Methane Hydrate Reservoirs by Numerical Simulation

Heriot-Watt University

School of Energy, Geoscience, Infrastructure and Society

Institute of Petroleum Engineering

Supervisor Dr. Karl D. Stephen

DECLARATION:

I Juan Tomasini confirm that this work submitted for assessment is my own and is expressed in my own words. Any uses made within it of the works of other authors in any form (e.g. ideas, equations, Figures, text, tables, programs) are properly acknowledged at the point of their use. A list of the references employed is included.

Signed……………………………………………..

Date……………………………………………….. 4/Nov/2017

ACKNOWLEDGEMENTS

The author would like to thank the National Energy Technology Laboratory from the U.S. Department of Energy for providing the simulator HydrateResSim and specially Ray Boswell, Yongkoo Seol and Evgeniy Myshakin for their help with the FORTRAN compilation of the simulator.

Additionally the author would like to thank project supervisor Dr. Karl D. Stephen for his continuous support and valuable insights during the project.

ANCAP, PGS, TOTAL and SHELL are acknowledged for their permission to use of seismic data in this project.

SUMMARY

In this work the potential for gas production from selected methane hydrate deposits offshore Uruguay is assessed. Specifically, after identification and ranking of methane hydrate reservoirs, the response during a field test was quantified by means of numerical simulation for two of the best ranked prospects.

Seismic interpretation was undertaken on the entire available dataset of 3D seismic acquired offshore Uruguay between 2012 and 2014 (approximately 38,500 km^2) for the identification of interest areas for gas hydrate studies. Due to the lack of well data at the selected locations, geological models and reservoir properties were defined based on published data from studies on analogue situations. The open source code freeware HydrateResSim developed at the Lawrence Berkeley National Laboratory of USA (Moridis, Kowalsky, and Pruess 2005) was utilized for modelling the response of selected prospects to depressurization induced dissociation.

Two prospects interpreted as turbidite type deposits located at 1850 m and 788 m of water depth were selected for the simulation studies. The simulation of short term production tests of 9 days indicates average gas release rate values from 55,000 Sm^3/d to 23,000 Sm^3/d for the deeper and shallower prospect respectively. A longer term production regime (180 days) was also simulated for the deeper prospect resulting in average gas release rate of 85,000 Sm^3/d, which is a very interesting value considering the average daily gas imports of Uruguay, indicating that only a few wells would be needed in order to satisfy the country current gas imports.

For the first time, reservoir simulation was applied for prospects in Uruguay. Simulations results are encouraging. Additionally, identified prospects may be useful for site selection for any future campaign for gas hydrate exploration offshore Uruguay.

TABLE OF CONTENTS

LIST OF ABBREVIATIONS

BSR: Bottom Simulating Reflexion

GHSZ: Gas Hydrate Stability Zone

HBL: Hydrate Bearing Layer

HCA: High Confidence Area

mbsf: meters below sea floor

NETL: National Energy Technology Laboratory

STP: Standard Temperature and Pressure

TVD: True Vertical Depth

TWT: Two Way Travel Time

GLOSARY

b: van Genuchten parameter

c: van Genuchten parameter

k_{rw}: relative permeability to water phase

k_{rg}: relative permeability to gas phase

λ: van Genuchten exponent

N/G: Net to Gross ratio

ø: porosity

P: Pressure

P_{cap}: capillary Pressure

P_o: van Genuchten pressure factor

Q_P: volumetric rate of CH_4 produced

Q_R: volumetric rate of CH_4 released from the dissociation

r_e: external radius

r_w: well radius

S_e: effective water saturation

S_g: gas saturation

S_H: hydrate saturation

Sm^3: standard cubic meter

Sm^3/d: standard cubic meter per day

S_w: water saturation

S_{w_max}: maximum water saturation

S_{wir}: irreducible water saturation

T: Temperature

V_R: cumulative volume of CH_4 released from the dissociation

z: vertical depth in m (negative and decreasing downwards)

1. AIMS AND OBJECTIVES

The aim of this project is to assess the potential for gas production from gas hydrate deposits offshore Uruguay. Specifically, the objective is to identify and rank methane hydrate reservoirs and quantify by means of numerical simulation the response of the best ranked prospects during a field test by depressurization induced dissociation.

Gas hydrate prospects were identified based on recently acquired 3D seismic and geological models were built for two selected prospects. Based on published data regarding reservoir properties from analogous accumulations; numerical reservoir simulation was applied in order to determine gas release rates. Additionally, the influence of key parameters like permeability and hydrate saturation was studied. A longer term production regime (180 days) was also performed for one of the selected prospects.

There have been no commercial hydrocarbon discoveries yet in the country; nevertheless unconventional reservoirs in the form of marine methane hydrate accumulations have been inferred from seismic data thus representing an important hydrocarbon resource for Uruguay. Considering current international research efforts towards the development of this kind of reservoirs, the analysis of the production behaviour is paramount to understand the real potential of gas hydrates offshore Uruguay.

2. INTRODUCTION AND LITERATURE REVIEW

Gas Hydrates

Gas hydrates are crystalline solids formed by gas and water, in which gas molecules are accommodated within a solid water lattice in a cage-like structure (Sloan 1998). They form in thermobaric conditions of relatively high pressure and low temperature which in nature occur in permafrost and deep water sediments environments. Within the solid crystalline structure, gas molecules are held close together, therefore gas is effectively compressed approximately 164 times by volume (STP) (Johnson and Max 2017)

As the future replacement of oil and specially coal, the use of natural gas will have the effect of lowering CO_2 emissions and it probably will emerge as the preferable fossil fuel backstop for renewable energy and the transition to it (Max and Johnson 2016). The amount of natural gas stored in the form of natural gas hydrate is really vast, largely surpassing the recoverable conventional natural gas (Moridis et al. 2009, Kvenvolden 1988). Being the estimation of the amount of gas being so high, even if a small portion result to be producible, the resource would be extremely important (Dillon and Max 2003). Natural gas hydrates have therefore the potential to be the natural gas source of the future.

International research on gas hydrates has grown exponentially in the past 20 years (Chong et al. 2016) and several countries have created specific national programs for hydrate research (Max 2006).

The first indication of the existence of natural gas hydrates is based on the presence of bottom simulating reflexions (BSRs) that arises from the high contrast in acoustic impedance between hydrate bearing layers (HBLs) and the free gas zone underneath. BSR indicates the base of the gas hydrate stability zone (GHSZ), nevertheless it does not give information regarding gas hydrate concentration in a volume of sediment (Max 2006).

Gas hydrate reservoir classification is based on the combination of phases found within and below the GHSZ. In a Class 1 deposit, gas is present below the base of the GHSZ in a two phase fluid zone (mobile gas) while in a Class 2 deposit, mobile water is present below the base of the GHSZ. On the other hand, Class 3 hydrate deposits presents only the hydrate bearing zone with no underlying mobile fluids (Moridis and Collet 2003). Usually Class 3 deposits are composed by HBLs confined between impermeable (water bearing) layers within the GHSZ. Research focus has gradually shifted from Class 1 (initially the most promising type due to favorable thermodynamic conditions, but likely rare in nature) to Class 3 type (Boswell et al. 2017).

Geological-Oceanographic Setting and Identification of Gas Hydrates Offshore Uruguay

Uruguayan continental margin is located between latitudes 34-38ºS, and between longitudes 50-56ºW. With an area of approximately 130.000km^2, it presents three basins: *Punta del Este*, *Pelotas* and *Oriental del Plata*. These basins were generated by the fragmentation and break-up of the Gondwana supercontinent and the subsequent opening of the Atlantic Ocean (Morales et al. 2017, Soto et al. 2011). At present times, the continental margin is characterized by the important input of large amounts of sediments from the Río de la Plata (Giberto et al. 2004) and by strong contour currents (Hernández-Molina et al. 2016).

Offshore Uruguay, different currents and water masses coexist playing an important role for the presence of methane hydrates considering, salinity, temperature and pressure conditions as well as sediment erosion and deposition. The complex interaction between several currents affects sedimentary processes and margin morphology. Large Contouritic Depositional Complex, including several kinds of erosive and depositional sedimentary features are created by the existence of strong contour currents (Hernández-Molina et al. 2016). These along slope processes coexist and interact with down slope depositional sedimentary gravitational processes related to series of submarine channels.

First identification of gas hydrates offshore Uruguay is reported in the work of (De Santa Ana et al. 2004), where the presence of a BSR is recognized on 2D seismic sections. Furthermore, other researchers interpreted the presence of gas hydrates based on this seismic feature on seismic data acquired in the study area (Neben et al. 2005, Tomasini et al. 2011, Gray 2014, Lavis, Huuse, and Thompson 2017) and additionally high methane concentrations and Anaerobic Oxidation of Methane within the upper few meters of sediments also suggest the existence of methane hydrate (Hensen et al. 2003).

There have been no commercial hydrocarbon discoveries yet in Uruguay, therefore identified unconventional gas reservoirs in the form of gas hydrate accumulations represents an important hydrocarbon resource for the country. The total volume of natural gas imported by Uruguay in 2016 corresponds to 62.4 million Sm^3 (DNE-MIEM 2016) which is equivalent to a daily average of approximately 171,000 Sm^3/d.

Production from Gas Hydrates

Gas production from gas hydrates is based on the induction of dissociation by one (or combination) of three methods: (1) depressurization, by lowering pressure below the hydration pressure; (2) thermal stimulation, by raising temperature above hydration temperature; and (3) by changing the P-T equilibrium curve using inhibitors such as salts and alcohols (Makogon 1997). An important difference with other producing conventional or unconventional gas reservoirs is the phase change (from solid to gas and liquid) that is needed to occur within the pore space. Additionally, dissociation is a strong endothermic chemical reaction and therefore a temperature reduction takes place during this process. Due to this reaction, during gas production also large amounts of water are released.

Studies regarding the suitability of these methods on different types of gas hydrates deposits showed that depressurization induced dissociation seems to be the most promising strategy for all classes (Moridis et al. 2009). In 2007, a short duration test was performed using the Schlumberger's MDT wireline tool on Mount Elbert (North Slope of Alaska). Additionally, other long term tests such as the one performed on Mallik-Canada in 2007 and 2008 (Dallimore et al. 2012) and on Alaska North Slope during 2011 and 2012 (Boswell et al. 2016) have proved the feasibility of depressurization method for gas production, and for the first time, from marine methane hydrates on 2013 from offshore Japan (Konno et al. 2017). Recently, also a gas production test from marine gas hydrates has taken place in the South China Sea (IHS_Energy 2017).

Given the unique aspects of natural gas hydrate deposits (in ultra-deep water but relatively shallow reservoirs of 1.2 km or less with temperatures below 30ºC), high capability drill-ships are not needed and new perspectives have to be explored (Johnson and Max 2017), i.e. shallow drilling units like MARUM-MeBo (Freudenthal and Wefer 2013). Technology development towards this kind of "light-weight" solutions may lead to the commercial development of natural gas hydrates (Max and Johnson 2016).

Gas Hydrate Reservoir Simulation

Numerical simulations to estimate the response of hydrate reservoirs to hydrate destabilization constitute a low-cost method that contribute to the planning, execution and study of the results of field production tests (Myshakin et al. 2017). The evaluation of the production potential from gas hydrates involves the interaction of complex coupled processes that occur during the dissociation reaction which cannot be solved by analytical models for long times, therefore numerical simulation is virtually the only tool that permit the assessment of the potential of gas hydrates reservoirs for gas production (Moridis et al. 2009).

Simulation of the behaviour of reservoirs containing gas hydrates involves the solution of complex combination of coupled equations for fluid, heat and mass transport (Wilder et al. 2008). Simulators should handle multiphase and multicomponent situations and because gas hydrate is a solid phase as well as ice, they need to take into account the possibility of solid phase formation and disappearance. These solid phases have an important effect on reservoir relative permeabilities and capillary pressures therefore impacting fluid flow (Moridis et al. 2009).

Gas hydrate reservoir numerical simulators have evolve significantly during the past years, mainly due to the availability of detailed reservoir information from gas hydrate deposits acquired by drilling programs around the world, which has led to better reservoir characterization (Boswell et al. 2017). There are several simulation code options available, being the following the most cited on scientific literature:

- CMG STARS from Computer Modelling Group (CMG 2017)
- HydrateResSim open source distributed by the National Energy Technology Laboratory (NETL) of USA (Moridis, Kowalsky, and Pruess 2005)
- MH21-HYDRES developed by the Japan Oil Engineering Company, the University of Tokyo and the National Institute for Advanced Industrial Science and Technology of Japan (MH21 2002)
- STOMP-HYD developed by the Pacific Northwest National Laboratory of USA (White and Ostrom 2006)
- TOUGH+HYDRATE, an updated version of HydrateResSim (Moridis, Kowalsky, and Pruess 2012).

Every production test performed was history matched with some gas hydrate reservoir simulator. Numerical history matching of the Mallik field test was performed by single-well radial model utilizing CMG-STARS (Uddin et al. 2012) while Alaska North Slope test was history matched with CMG-STARS, HydrateResSim, MH21-HYDRES, STOMP-HYD, and TOUGH + HYDRATE (Anderson et al. 2011). On the other hand MH21-HYDRES simulator was used to history match results from the offshore test performed in Japan (Konno et al. 2017).

From the common simulators options mentioned above, only the HydrateResSim is a freeware (NETL 2017) and therefore this has been the option chosen for this work as an initial approximation to the problem.

HydrateResSim is an open source code written in FORTRAN95/2003, developed at the Lawrence Berkeley National Laboratory (Moridis, Kowalsky, and Pruess 2005). It is based on the family of codes TOUGH2 for the simulation of the behavior of hydrate - bearing geologic systems. The code can model non-isothermal gas release, phase behavior and flow of fluids and heat at common conditions of natural methane hydrate accumulations. More details regarding HydrateResSim can be found in Appendix A.

3. DATA SUMMARY

Data used for the identification, delineation and selection of prospects corresponds to 3D seismic surveys acquired offshore Uruguay between 2012 and 2014. The entire available 3D dataset corresponds to approximately 38,500 km^2. ANCAP (the national oil company) owns all seismic data which was acquired under different multi-client and proprietary contracts offshore Uruguay. Given the confidential nature of the information, specific authorization was obtained for its use on this project.

Most of the surveys have some kind of depth conversion and when available, the interpretation was performed on depth converted data instead of two way travel time (TWT). Location and details of seismic surveys used in this work are presented in Fig. 1 and Table 1 respectively.

4. METHODS USED

4.1 Prospect selection

At the stage of prospect selection, 3D seismic data analysis was performed by the use of IHS Kingdom Software 2016.1 from ANCAP`s seismic server. Based on the known characteristics of BSRs, interpretation was undertaken on the entire 3D dataset for the identification of interest areas for gas hydrate studies. Only clear BSR cases were considered, therefore these locations are named as “High Confidence Areas” (HCAs). For each HCA, the geological setting and type of deposits was interpreted in order to assess the expected reservoir quality of any distinct body interpreted within the GHSZ. For the geological interpretation of the shallow portion of the GHSZ, the work of (Hernández-Molina et al. 2016) was used as a reference guide.

Present day technologies make production from gas hydrate deposits possible by using conventional approaches only for sand type reservoirs (Moridis et al. 2009), therefore this work was focused on finding high reservoir quality prospects.

A qualitative criterion was used in order to assign expected reservoir quality to each type of deposits. This criterion is presented in Table 2 and corresponds to “High” reservoir values for the case of Turbidite deposits to “Low” reservoir values for the case of Contourite Drifts and Mass Transport Complexes.

Based on gross reservoir thickness and expected reservoir quality, a prospect ranking was constructed. The top-most prospects were selected for this study.

4.2 Validation of the simulator

The HydrateResSim version received from NETL was validated for a depressurization induced dissociation case within a single layer in a 2D Cartesian model known as “*Problem Test_2D: Equilibrium Hydrate Dissociation, 2-D Areal System*” in (Moridis, Kowalsky, and Pruess 2005). Results are presented in Appendix B revealing that the available simulator provides gas release rate values higher than the values presented in (Moridis, Kowalsky, and Pruess 2005). Being the difference approximately 5% (for average values), simulator performance is considered to be validated for the purpose of the present study.

4.3 Simulation model

Due to the lack of well data at the selected locations, geological models and reservoir properties were defined based on published data from studies on analogue situations.

Studies that assess production potential by reservoir simulations includes areas offshore Japan (Kurihara et al. 2010) (Zhou et al. 2014) (Konno et al. 2017), offshore Korea (Moridis et al. 2013), offshore China (Su et al. 2010) and offshore USA (Gaddipati and Anderson 2012) (Myshakin et al. 2012) (Myshakin et al. 2017). These studies have been analyzed in order to define a dataset of properties and model parameters that could be applied to the selected prospects. Comparison of the different parameters used on each of these works is presented in Appendix C.

Geological and reservoir model

Considering analogue prospects from literature regarding turbidite deposits hosting gas hydrates, the geological model for selected turbidite prospects offshore Uruguay has been considered as layers of fine sand interbedded with clayey silt layers with variable thickness from tens of centimeters to few meters. In this work, permeable layers composed of fine sands are referred as “sand” layers while less permeable clayey silt layers are referred as “mud” layers.

For each selected prospect, a lithological profile for a hypothetical well was created considering layers of 0.2 m thickness. For each layer, using @Risk software, different lithofacies were assigned based on a discrete density probability function with probabilities of 70% for sand and 30% for mud layers. These values were arbitrary selected considering turbidite lobe type deposits, which are known to have high N/G ratios. According to (Fujii et al. 2015), N/G ratio of the turbidite deposit tested in the eastern Nankai Trough is 0.67. The resulting “synthetic” distribution of lithofacies for each prospect is presented in Appendix D.

In order to predict gas production rates from hydrate deposits, authors have applied both 3D (Kurihara et al. 2010, Gaddipati and Anderson 2012, Myshakin et al. 2012, Zhou et al. 2014) and 2D radial (Su et al. 2010, Myshakin et al. 2012, Moridis et al. 2013, Zhou et al. 2014, Konno et al. 2017, Myshakin et al. 2017) reservoir models. 3D models can provide more representative results when there is high variability in reservoir properties, including fractures, faults and dipping beds (Myshakin et al. 2012), but they imply a higher level of complexity than 2D models and may lead to various numerical problems. Numerical simulations performed by (Myshakin et al. 2012) for gas production from gas hydrate reservoirs by 2D and 3D models shows close agreement.

Zhou et al. (2014) make use of a simulator that takes into account the geomechanical behavior of hydrate bearing sediments, concluding that seabed slope does not significantly affect the dissociation, temperature and pore pressure, affecting only mechanical deformation. Is worth to mention that as many of the presented gas hydrate simulators, HydrateResSim does not take into account geomechanical behaviour of the reservoir during hydrate dissociation.

Therefore, and taking into account the lack of data regarding reservoir properties and its spatial variation, the geometry selected for modelling in this work corresponds to 2D radial RZ axisymmetric.

Borehole radius is considered to be $r_w = 0.15$ m (Zhou et al. 2014, Myshakin et al. 2017) and external radius r_e of approximately 100 m as well as on (Su et al. 2010) and to reach manageable running times. Due to convergence problems when applying logarithmic radial distribution, in the lateral direction, the simulation domain is uniformly divided into 33 grid-blocks of 3 m length. In the vertical direction, simulation domain includes approximately 5 m of sediments above and below the top and bottom of the producing interval respectively.

According to (Fujii et al. 2015), the presence of sealing layers below and above the production interval is critical for an effective depressurization as they prevent the water entering from the water-bearing layers. Therefore, as in the case of the production test offshore Japan, the bottom of drilling completion at the simulated well was set 20 m above the BSR.

The well bottomhole pressure is set to 3.0 MPa to exceed the CH_4-hydrate quadruple point pressure, therefore avoiding ice formation and the corresponding adverse effect of permeability reduction which may lead to complete flow blockage. Given the fact that the pseudo-porous medium approach used for wellbore modelling (Moridis and Reagan 2007a) led in this case to numerical problems, each grid cell corresponding to the wellbore subdomain was set at fixed conditions and only the layers thicker than 20 cm were open to production.

Permeability

Permeability is a critically important parameters that affects estimations of productivity. Intrinsic or absolute permeability corresponds to the permeability of the sediments when no hydrate is present, while effective permeability refers to the permeability when the hydrates and/or emerging gas phase are present within the reservoir. Recent results from pressure cores obtained from turbidite deposits offshore Japan (Konno et al. 2015) indicates that in situ effective permeability of sandy reservoirs may range from 1 to 100 mD which is 2-3 orders higher than previous estimations like at (Anderson et al. 2011).

Regarding intrinsic permeability, values for sandy reservoirs may range from 100 to 1000 mD but as stated by (Boswell et al. 2017) this parameter should consider the geomechanical effects of the dissociation of hydrates that may lead to compaction effects due to the disappearance of the solid phase. The magnitude of this effect will depend on sediment compaction and therefore on reservoir depth (which is controlled by water-depth).

According to (Konno et al. 2017), gas hydrate bearing sandy deposit tested offshore Japan consist of fine sands and very fine sands with absolute permeabilities ranging from 10 to more than 1000 md (interbedded sandy silt layers present permeabilities between 1 and 10 md approximately). Considering this, and taking into account that HydrateResSim does not considers the geomechanical effects associated with hydrate dissociation, the base case permeability for this study was stablished at 100 md for all sandy hydrate bearing layers. Sensitivity analysis was performed for 10 md, 500 md and 1000 md permeability cases. In all cases, the ratio between horizontal and vertical permeability was fixed at 10.

To facilitate convergence of the numerical solution, mud layers were considered as impermeable. Overburden sediments were considered in this work as low permeability layers (mud) with the same values as the interbedded low permeability layers.

Relative permeability model used in this work corresponds to (Van Genuchten 1980):

$$k_{rw} = {S_e}^b \left[1 - \left(1 - {S_e}^{\frac{1}{\lambda}}\right)^{\lambda}\right]^2 \qquad and \qquad k_{rg} = (1 - S_e)^c \left(1 - {S_e}^{\frac{1}{\lambda}}\right)^{2\lambda}$$

Being: $S_e = \frac{S_w - S_{wir}}{S_w + S_g - S_{wir}}$

Considering the updated parameters from (Zhou et al. 2014) regarding the calibrated model from eastern Nankai Trough site data:

$S_{wir} = 0.2$

$S_{gir} = 0.012$

$\lambda = 0.85$

$b = 0.62$

$c = 1.8$

Given the fact that HydrateResSim does not consider b and c parameters different from 0.5, the code was modified in order to take into account the updated values (see Appendix E with the code modification and resulting relative permeability curves). For the calculation of S_e, the original parameter S_{w_max} used at HydrateResSim code was maintained and assumed $S_{w\_max} = S_w + S_g = 1$.

Capillary pressure model, as in the majority of the mentioned sources, correspond to (Van Genuchten 1980) :

$$P_{cap} = -P_o \left({S_e}^{-1/\lambda} - 1 \right)^{1-\lambda}$$

A slight modification of the code was performed in order to set P_o as input parameter (see Appendix F).

In this case S_e is calculated with $S_{wir} = 0.19$. According to (Moridis et al. 2013), parameters used in this work correspond to:

λ: 0.45 (sand); 0.15 (clay/mud)

P_o: 10^4 Pa (sand); 10^5 Pa (clay/mud)

Petrophysical parameters

Based on the work from the mentioned sources, and especially considering the porosity and hydrate saturation profiles presented by (Konno et al. 2017), a unique porosity value of 40% was assigned to each grid cell, and a unique hydrate saturation of 60% was assigned to each sand layer.

Based on (Su et al. 2010) and (Myshakin et al. 2012), thermal conductivity of the porous media is considered to be 1 W/(mK) for dry case and 3.1 W/(mK) for the wet case (both for sand and mud layers).

Pore compressibility is considered to be $1x10^{-9}$ Pa^{-1} according to (Gaddipati and Anderson 2012) and (Myshakin et al. 2012).

Values of 2,750 kg/m^3 and 2,650 kg/m^3 for rock density were assigned for mud and sand layers respectively (Moridis et al. 2013). A rock grain specific heat of 1,000 J/(kg°C) was considered for every grid block (Gaddipati and Anderson 2012, Myshakin et al. 2012, Myshakin et al. 2017).

Hydrate properties

Equilibrium relationship between hydration pressure and the corresponding equilibrium hydration temperature can be obtained in HydrateResSim from two sources: (Moridis 2003) and (Kamath and Holder 1987). The latter one, corresponding to:

$$P = e^{\left(b_1 + \frac{b_2}{T}\right)}$$

Being:

P: equilibrium pressure in 10^3 Pa

T: equilibrium temperature in K

b_1: 38.980 (for 0°C < T ≤ 25°C)

b_2: -8,533.80 (for 0°C < T ≤ 25°C)

Considering a salinity of 35,000 ppm, (Zhou et al. 2014) presents updated parameters for the previous equilibrium equation: $b_1 = 39.10$ and $b_2 = -8{,}508$. Graphical comparison between both equilibrium curves is presented in Appendix G.

HydrateResSim can consider the effect of inhibitors like salt and alcohol on equilibrium P-T relationship, nevertheless the uncertainty on the required parameters and the simplicity of the Kamath equation updated for the corresponding seawater salinity led to the use of this method. For this reason the HydrateResSim code was modified as presented in Appendix G. Hydrate dissociation was considered as an equilibrium reaction (Kowalsky and Moridis 2007).

Pressure-Temperature conditions

Temperature at seafloor was obtained by using Ocean Data View (Schlitzer 2014) from World Ocean Atlas database,1 deg. grid, annual values (NOAA 2013). Selected data site corresponds to Station 12301 (B) with a depth range from 0 to 1900 m (Appendix H). Based on this temperature profile, seafloor temperature is assume to be 3.2 ºC at 1,850 m of water depth (prospect HP11-A) and 4.5 ºC at 800 m of water depth (prospect HP25).

Sediment temperature was calculated based on a geothermal gradient of 0.05537 ºC/m for prospect HP11-A and 0.03419 ºC/m for prospect HP25 (calculated based on the base of GHSZ depth and equilibrium curve from (Zhou et al. 2014). Therefore:

For prospect HP11-A: $T(z) = 3.2 - 0.05537\, z$

For prospect HP25: $T(z) = 4.5 - 0.03419\, z$

Seawater salinity was considered at 35,000 ppm and a mean temperature of 10 ºC was assumed in order to use a mean water density of 1.027 g/l (Millero and Poisson 1981) for pressure gradient calculations, resulting in 0.01007 MPa/m (0.445 psi/ft).

For prospect HP11-A: $P(z) = -0.01007\, z + 18.63$

For prospect HP25: $P(z) = -0.01007\, z + 7.93$

Being:

z: vertical depth in m (negative and decreasing downwards)

P: pressure in MPa

T: temperature in ºC

Top and bottom layers were set at Dirichlet fixed conditions. Lateral boundary conditions correspond to no flux Neumann conditions, which is the default in the integral finite difference framework when no flow connections are prescribed across the boundary (Moridis, Kowalsky, and Pruess 2005). A schematic of the models considered for both prospects is presented in Fig. 4.

A summary of the simulation model parameters is presented in Appendix I

4. RESULTS

This chapter covers the results obtained from the prospect selection process as well as the numerical simulations performed.

Prospect selection results

As a result from the interpretation of BSRs from the 3D seismic dataset, a total of 39 HCAs were identified.

For each of these HCA, the geological setting was interpreted resulting in six different types of deposits: (1) Mass Transport, (2) Contouritic Drifts, (3) Contouritic Terraces, (4) Shelf to Slope Progradations, (5) Channel Fill and (7) Turbidites.

During the interpretation of the geological setting, some HCA were subdivided, creating new interest zones (i.e. 15-A, 15-B, 15-C). A total of 46 zones were studied. Details of each accumulation are presented in Appendix J.

During this process, based on geometry and seismic attributes (i.e. blanking), eight distinct geological bodies were interpreted on different geological settings. These exploratory situations were considered as prospects.

In order to construct a prospect ranking, expected reservoir quality and reservoir thickness were considered. Expected reservoir quality was evaluated based on the arbitrary criteria presented in Table 2. As a result, prospects were classified as two High, three Medium-High and three Low expected quality reservoirs. Reservoir thickness ranges from 38 to 160 m. Prospect ranking presenting reservoir gross thickness and expected quality is presented in Table 3.

The highest ranked prospects (HP11-A and HP25) were selected for the application of numerical simulation studies.

Considering that the highest hydrate saturation is expected to be in the proximity of the base of the GHSZ (indicated by the BSR) and in order to cover the highest possible reservoir thickness within the hydrate stability zone, the wells modelled on each prospect were located at the intersection of the base of the interpreted reservoir unit and the BSR. Selected seismic sections of each prospect are presented in Fig. 2 and Fig. 3.

Prospects HP11-A and HP25 correspond to possibly plio-pleistocene turbidite type deposits located at approximately 1850 m and 788 m of water depth respectively (at the selected well locations).

Gross reservoir thickness at the selected well locations for prospects HP11-A and HP25 are 60 and 64 m respectively, which are comparable with 60 m gross thickness of the methane hydrate concentrated zone of the turbidite reservoir tested in eastern Nankai Trough (Konno et al. 2017).

Prospect HP25 is interpreted to have an area of approximately 31 km^2, while prospect HP11-A has an area of approximately 20 km^2. According to (Fujii et al. 2015), methane hydrate concentrated zone tested in Nankai Trough is interpreted to have an area of approximately 12 km^2, which is in the order of selected prospects in this work.

Reservoir Simulations Results

Simulation results for the base case scenario (100 md) are presented at Fig. 5 including gas release rate (Q_R) in Sm^3/d and cumulative gas volume released (V_R) in million Sm^3 for a 60 days period. Mean gas release rates correspond to approximately 126,000 Sm^3/d and 82,000 Sm^3/d for prospects HP11-A and HP25 respectively. For prospect HP11-A, maximum release rate reaches values higher than 290,000 Sm^3/d while for prospect HP25 maximum release during the simulated time reaches values of approximately 150,000 Sm^3/d. Cumulative gas volumes correspond approximately to 7.0 million Sm^3 and 4.4 million Sm^3 for prospects HP11-A and HP25 respectively.

For prospect HP11-A, a long term simulation was performed reaching 180 days. Results are presented in Fig. 6. In this case, approximately after day 55, a decline phase is observed, reaching Q_R values of approximately 27,000 Sm^3/d and V_R of 14 million Sm^3 at day 180. The spatial distribution of selected parameters is presented in Fig. 7 for 30 days (before maximum rate), 55 days (at maximum rate) and 180 days (after maximum rate).

Different permeability scenarios were also explored for a period of 30 days of simulation for both prospects. To facilitate visualization, on graphs related to sensitivity analysis, Q_R values are plotted according to a one day sampling interval. For prospect HP11-A, results regarding gas release rate and cumulative gas volume released are presented in Fig. 8. Results for prospect HP25 are presented at Appendix K.

For prospect HP11-A, the spatial distribution of selected parameters is presented in Fig. 9 for three permeability scenarios at 30 days of simulation time.

Three different scenarios regarding gas hydrate saturation were also explored for prospect HP11-A and results are presented in Fig. 10.

5. DISCUSSION

Seismic interpretation and prospect selection

At the interpretation and prospect selection phase of this work, only high confidence areas were considered. There may be other situations where BSR is not so clear but geological setting is such that high reservoir quality could be inferred within GHSZ.

Only two prospects were selected for simulation studies, these prospects were interpreted as turbidite deposits. Moreover others high thickness channel fill type prospects may represent additional interesting prospects (i.e. HP8-D and HP22-A, see Table 3).

Gas hydrate deposit classification and associated production behaviour

For the selected well position, studied prospects were classified as Class 3 gas hydrate deposits, nevertheless considering the relative depth of the base of the reservoir interval regarding to the base of the GHSZ, prospects could be classified as a mixed case with class 2 (or even with class 1) at the updip region (from where the BSR cross the base of the turbidite lobe). This can be observed at the left hand side of the “Simulated Well” at Fig. 2 and Fig. 3. Taking this into account is probable that production and reservoir behaviour to depressurization will be different among these two regions at the long term if the fluids underneath the base of GHSZ (gas or water depending on the class) reach the completion interval. Nevertheless the completion strategy considered in this work regarding the distance between the bottom of the completion and the base of GHSZ avoid the destabilization of the lower HBLs and the mayor difference with the simulated well would be the thinning of the hydrate bearing interval when moving to an updip position and the different pressure and temperature conditions.

Available outputs and simulator performance

The available version of the simulator does not deliver the complete set of outputs reported on its manual and it was confirmed that other users experience the same issue. Given the fact that it is a freeware, open-source code for use “as-is”, there is no user or technical support available, therefore and despite several tests and revision of source code files, the author have not yet arrive to an explanation for these missing outputs. Nevertheless the simulator performance was validated for Q_R and V_R as presented in section 4.2.

Given the fact that nor the *Conx_Time_Series* file (for the reporting of connections fluxes) or the *SS_Time_Series* file (for the reporting of the sink cells fluxes) were functional in the available HydrateResSim version, the determination of the production potential was based on the information given by the *Hydrate_Info* file. This output file provides a measure of the overall performance of the hydrate-bearing system as a gas production source (Moridis, Kowalsky, and Pruess 2005). The reported output corresponds to the volumetric rate of CH_4 released from the dissociation (Q_R). Additionally, the cumulative volume of CH_4 released from the dissociation (V_R) is also reported. At the beginning of the dissociation process, Q_R should exceed gas production (Q_P) until enough gas is released in the system and gas saturation reaches the irreducible value to allow the start of the production. Nevertheless, as found by (Moridis and Reagan 2007b), during the production, quite often Q_P exceeds Q_R indicating a support to the production from stored gas that was previously released. After exhausting the hydrate, Q_R falls to cero while the production is entirely supported by the stored gas (Moridis and Reagan 2007b), furthermore these authors conclude that at the end of their simulation time (6000 days for their model), the total gas volume produced is 99% the total gas volume released. Therefore the average Q_R over the simulation time was taken as an approximation to the average Q_P of the well. According to (Myshakin et al. 2012), one of the mayor challenges in simulations from gas hydrates reservoirs is given by the secondary hydrate formation in the vicinity of the well which require smaller time steps to achieve convergence and could cause numerical errors. In the case of the present work numerical convergence was really challenging and was no possible to use logarithmic radial grid discretization, high radial extension or longer simulation times.

Impermeable mud layers

Overburden and other mud layers were considered as impermeable due to convergence problems arising when using permeable mud layers. Regarding gas production, the adverse effects of permeable confining layers would be related to additional water entering the reservoir due to the pressure reduction and the escape of gas due to buoyancy. According to (Myshakin et al. 2012), the effect of confining layer`s permeability on cumulative volume of gas produced is observed after approximately 70 days, therefore for the short time simulated in the present work, the effect is not expected to be appreciable.

Production behaviour and model's lateral extension

The behaviour of the gas release rate profile shows several ups and downs which are typical for the depressurization dissociation induced method due to the formation of barriers of secondary hydrate (Moridis et al. 2009). Secondary hydrate formation is observed in the spatial distribution figures that shows hydrate saturation in Fig. 7 and Fig. 9 where can be observed that hydrate saturation reaches values higher than the original value of 60% and this have the effect of reducing the effective permeability close to the wellbore stopping the gas flow from certain layers.

Nevertheless, ups and downs in early production are interpreted to be not only because secondary hydrate barrier formation but because the hydrate dissociation front reaches the model boundary at different times for each layer. Every time the hydrate dissociation front reaches the boundary at a particular layer its gas release rate starts to decline but at different times other layers are starting to release increasingly rates of gas to the system. Once the hydrate dissociation front reaches the model boundary at the majority of the layers, a decline phase starts. As can be observed in Fig. 7, even at the declining phase at 180 days some layers still have zones with the original hydrate saturation. That indicates the possibility of small increases in the gas release rate after that time.

The effect of the lateral extension of the model is then evident and the selection of external radius (r_e) may have big effect and important implications in the gas release rate profile. In this case r_e = 100 m was used to solve convergence problems and reduce simulation time, hence hydrate dissociation front reaches the 100 m boundary very early in time (approximately at 9.5 days for prospect HP11-A and 20 days for prospect HP25 as presented in Appendix L). Therefore to obtain representative values for a short production test, only the behaviour from early times (before hydrate dissociation front reaches model boundary) should be considered. As presented in Fig. 5, for a 9 day test, release rates for both prospects are closer than in the long term, but still prospect HP11-A has a better performance than prospect HP25 (55,000 Sm^3/d and 23,000 Sm^3/d respectively, being average values from start of the simulation).

Comparison with field tests

Available information for the only two tests performed for gas production from marine natural gas hydrate deposits indicates average values of 20,000 Sm^3/d for a 6 day period in Japan (Konno et al. 2017) and 5,000 Sm^3/d for a 60 day period in China (IHS_Energy 2017). At the time the present work was performed, no peer review publications were available regarding the test from China. On the other hand, long term simulations performed by (Konno et al. 2017) based on the field test data from Japan shows, for 180 days, maximum values of 90,000 Sm^3/d without reaching any peak (r_e=5000 m). Even with several differences between models (see Appendix C) these values are in the order of magnitude to the results obtained in the present work.

Comparison of production potential between prospects

As presented in Fig. 5 prospect HP11-A presents a better reservoir performance in terms of gas release rate and cumulative gas release compared with prospect HP25 (even when completion interval in prospect HP25 is almost 4 m longer than for prospect HP11-A). This difference is attributed to the particular thermobaric conditions for each prospect and specially reservoir temperature that is higher at the deepest prospect (HP11-A) providing extra source of heat for the endothermic dissociation reaction compared with reservoir temperature at prospect HP25. Additionally, regarding reservoir pressure, drawdown for prospect HP11-A is higher than for prospect HP25. Geomechanical effects of dissociation were not modeled as is not possible with the available simulator software, nevertheless considering sediment consolidation is possible that the deepest prospect will behave better from the geomechanical point of view as well (smaller effect on intrinsic permeability and lower probability for sand production).

Economic factors were not considered at this stage. HP11-A as deeper reservoir will represent higher development costs and it should be studied if the higher production is enough to generate enough revenue to make its development feasible from the economic point of view.

Sensitivity analysis

Sensitivity analysis was performed for four permeability scenarios for each prospect and for three hydrate saturation scenarios for prospect HP11-A. According to (Wang et al.

2016), production behaviour is not sensitive to thermal conductivity, therefore no sensitivity analysis was performed for this parameter.

The result of the sensitivity analysis for permeability shows that for higher values of permeability, the system reaches the peak release rate early (Fig. 8). During the 30 day period for comparison, for both prospects, permeability scenarios 10 md and 100 md shows increasing release rates while scenarios for 500 md and 1000 md shows already declining release rates (the peak occur before 30 days). For the case of 1000 md, high amounts of gas are released very early in the simulation time (more than 3,000,000 Sm^3/d at the peak), consequently there is a strong decline phase after reaching the peak. In this case, due to this strong decline, at some point before the 30 days period of comparison, release rate values for the 1000 md scenario are surpassed by the 500 md scenario rate values.

As can be observed in Fig. 9, for the 1000 md scenario, at 30 days, reservoir pressure has reached bottomhole pressure (3 MPa) in almost all the layers. Due to the strong endothermic nature of the hydrate dissociation reaction, reservoir temperature experiences an important decrease, especially in the bottommost layers with values close to 1.2 ºC. Hydrate saturation values decrease to approximately 30% and gas saturation reach values of approximately 10%.

On the other hand, the spatial distribution for the 10 md permeability scenario show that only a few of the bottommost layers present some degree of dissociation at 30 days, that explain the very small gas release rate values obtained for this scenario.

Sensitivity analysis to hydrate saturation was performed for 40%, 60% (base case) and 70% values and results are presented in Fig. 10. Results shows higher Q_R values for the S_H = 40% case scenario reaching the peak at early times (before 20 days). In this case the lower hydrate saturation has a positive effect on the relative permeability and consequently pressure disturbance front can move faster inducing gas hydrate dissociation in all the HBL at early times compared with the base case. Cumulative gas release is higher for the 40% case compared with the 60% base case at 30 days, nevertheless this behaviour is expected to revert at some moment in time considering that the total amount of gas in the system is higher for the latter.

On the other hand the 70% scenario results in very low relative permeability values and consequently gas release rate is marginal.

Geological model

The model has considered only two types of lithology (sand and mud) with a specific interlayering, considering impermeable mud layers. Nevertheless the actual prospect may be most certainly formed by several types of sand and mud units with different permeability and hydrate saturation values. The combination of different sand layers with different permeability, hydrate saturation and thickness values will result in different speed of the pressure disturbance and hydrate dissociation fronts affecting the gas release rate profile. More information is needed from the prospects in order to generate a more accurate reservoir model (i.e. well logs and cores).

The geological model selected for each prospect is only one of many possible cases. Due to the time consuming characteristics of the model loading process, no sensitivity analysis was performed for this aspect of the study and this could be subject of further work.

Given the results regarding the strong cooling effect by the endothermic reaction, the simplification by using 1D models is not recommended due to the important thermal interaction found between layers. In other words, the dissociation behaviour of each layer is not only conditioned by the pressure disturbance from the wellbore but by the reservoir temperature resulting from the different stages of dissociation from other layers (which is also conditioned by layer thickness). For longer simulation times and permeable mud layers, pressure differences from adjacent layers will also contribute to the dissociation behaviour of each layer.

Long term simulation and gas rates for the Uruguayan market

Long term simulation presented in Fig. 6 indicates an average gas release rate of 85,000 Sm^3/d for prospect HP11-A which is a very interesting value considering the average daily gas imports of Uruguay (approximately 171,000 Sm^3/d according to 2016 values) (DNE-MIEM 2016). These results indicates that only a few wells would be needed in only one hydrate prospect in order to satisfy the country current gas imports. Additionally, the effect of boundary conditions discussed above suggests that long term production rates may be even higher.

6. CONCLUSIONS

- Offshore of Uruguay presents several prospects for methane production from methane hydrate reservoirs including turbidite type deposits with high potential for very good reservoir quality.
- The simulation of short term production tests of 9 days for two selected prospects indicates average Q_R values from 55,000 Sm^3/d to 23,000 Sm^3/d.
- Results are in the order of gas production rate values from actual production tests performed from methane hydrate deposits at different offshore basins in recent years.
- Long term simulation results indicate that only a few wells would be needed in one hydrate prospect in order to satisfy Uruguay’s current gas imports.
- By the comparison of reservoir behaviour in terms of gas release rate, the deeper prospect (1850 m of water depth) would be a better candidate for production than the shallower one (787.5 m of water depth). This is because of differences

in reservoir temperature and pressure but also because inferred difference in sediment compaction.

- The prospect ranking and simulations results may be useful for site selection for any future campaign for gas hydrate exploration offshore Uruguay. More information regarding lithology and reservoir properties is needed for the selected prospects, therefore the acquisition of well logs and cores would be the next step to enhance the understanding of this kind of deposits and re-evaluate its resource potential.

7. SUGGESTIONS FOR FURTHER WORK

- The use of a different simulator is recommended (i.e. TOUGH+HYDRATE). This will allow modeling sink cells and obtain additional important parameters like production rates and water/gas producing ratio.
- Perform full field simulations in order to cope with different classes of deposits within the same prospect and to address the issue of reservoir external radius. In other case, test different well locations within a prospect and set higher r_e (i.e. 1000 m) for the reservoir models.
- Perform sensitivity analysis to the geological model. Preferably, this should be done by coupling some Monte Carlo type simulation tool with the geometrical section of the simulator input file in order to assess the impact of a wide range of possibilities regarding the geological model.
- Perform pre-feasibility studies by technical-economic evaluations for the development of the studied prospects once new lightweight drilling and completion technology becomes available.

8. FIGURES AND TABLES

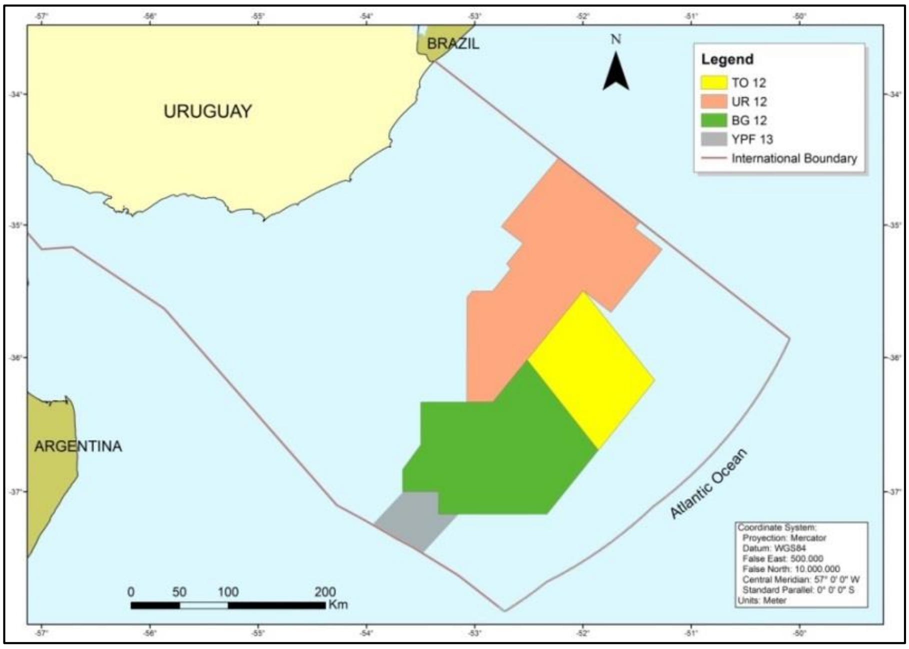

Fig. 1 – 3D seismic dataset

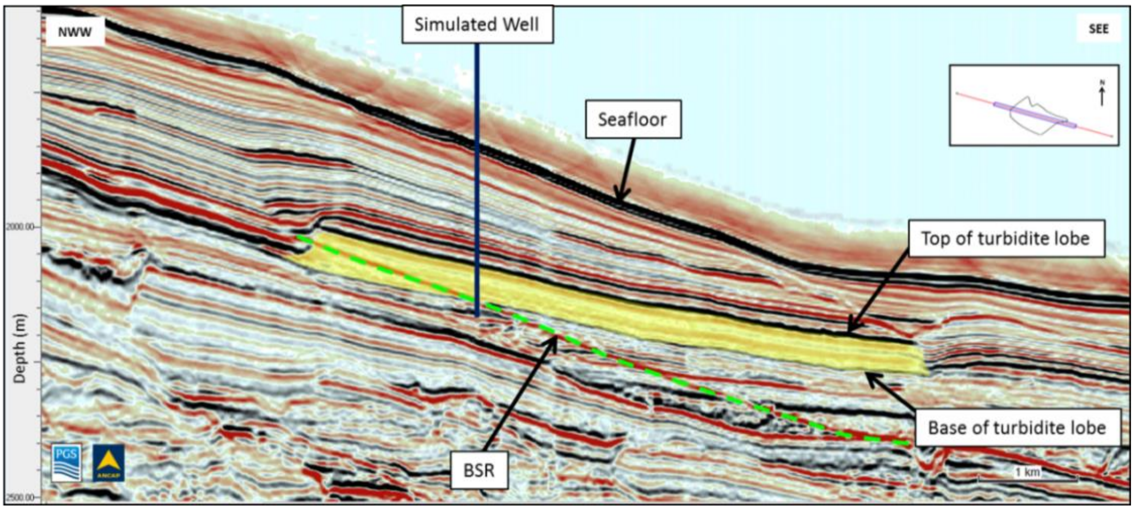

Fig. 2 - Seismic section showing prospect HP11-A. Interpreted reservoir unit is highlighted in transparent yellow and BSR interpretation is showed in dashed green line. Depth in m TVDss. PGS and ANCAP are acknowledged for their permission to disclose this seismic section.

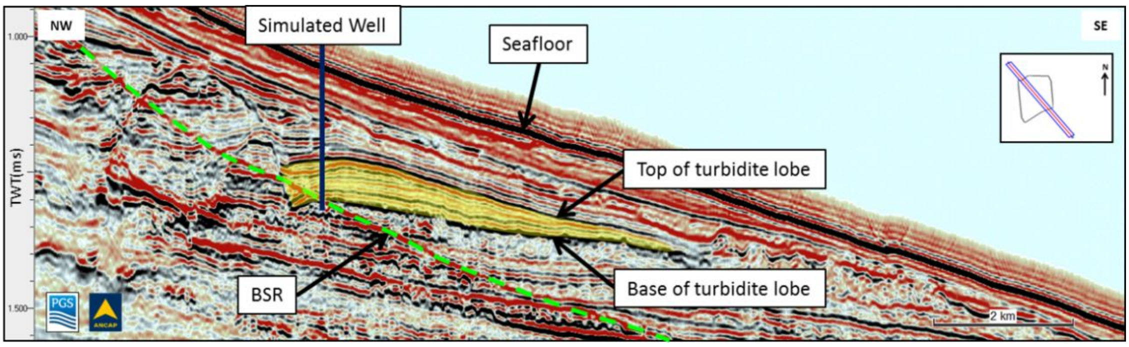

Fig. 3 - Seismic section showing prospect HP25. Interpreted reservoir unit is highlighted in transparent yellow and BSR interpretation is showed in dashed green line. Data in TWT(ms). PGS and ANCAP are acknowledged for their permission to disclose this seismic section.

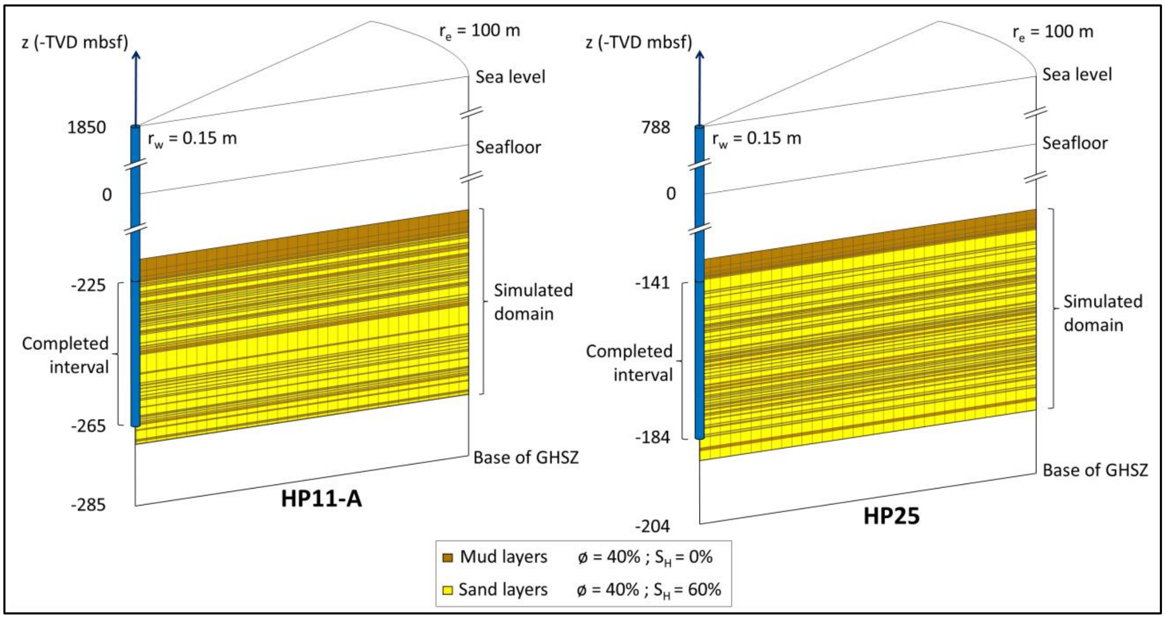

Fig. 4 – Schematics of simulated methane hydrate deposits

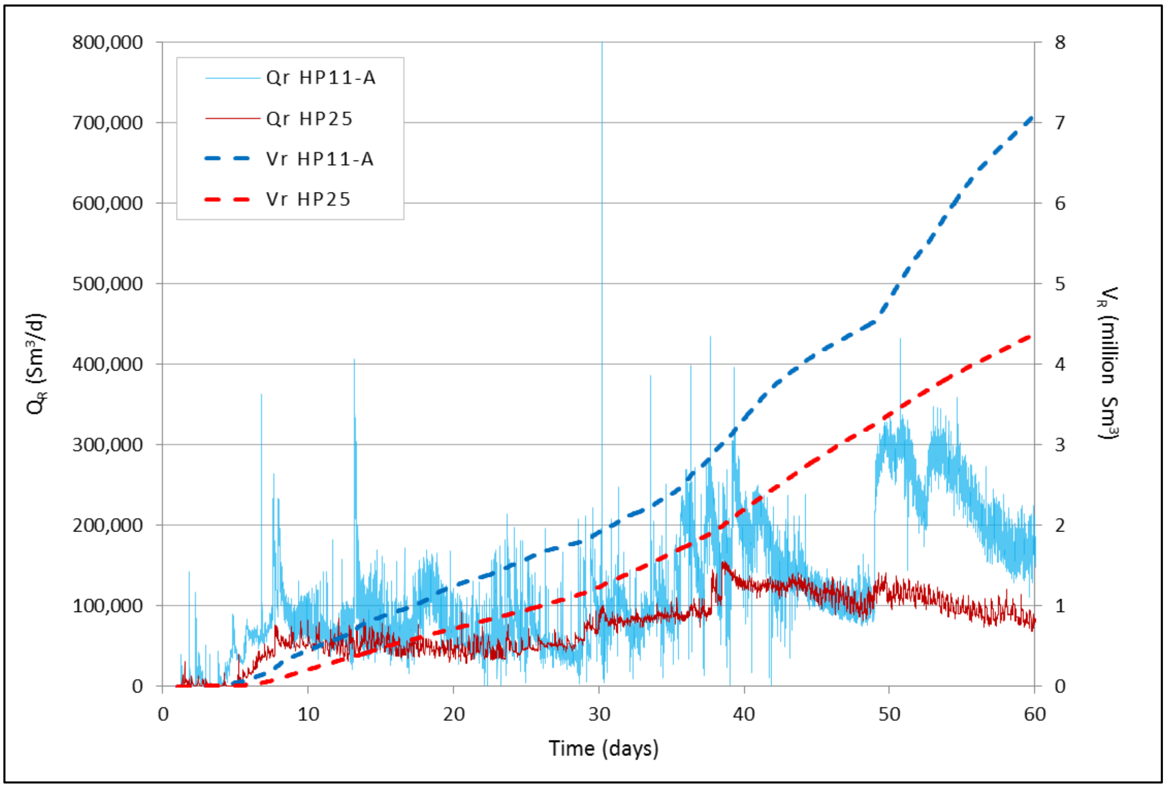

Fig. 5 – Gas release rate (Q_R) and cumulative gas released volume (V_R) for prospects HP11-A and HP25

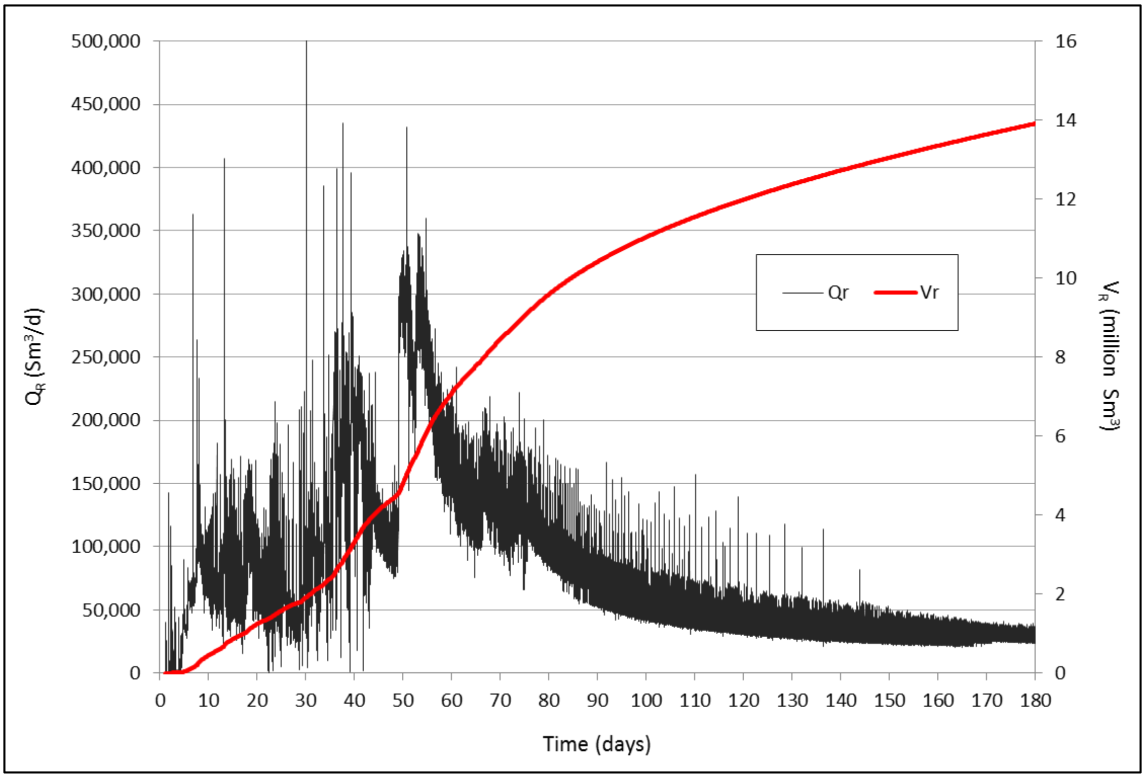

Fig. 6 – Gas release rate and cumulative gas volume for prospect HP11-A (long term simulation)

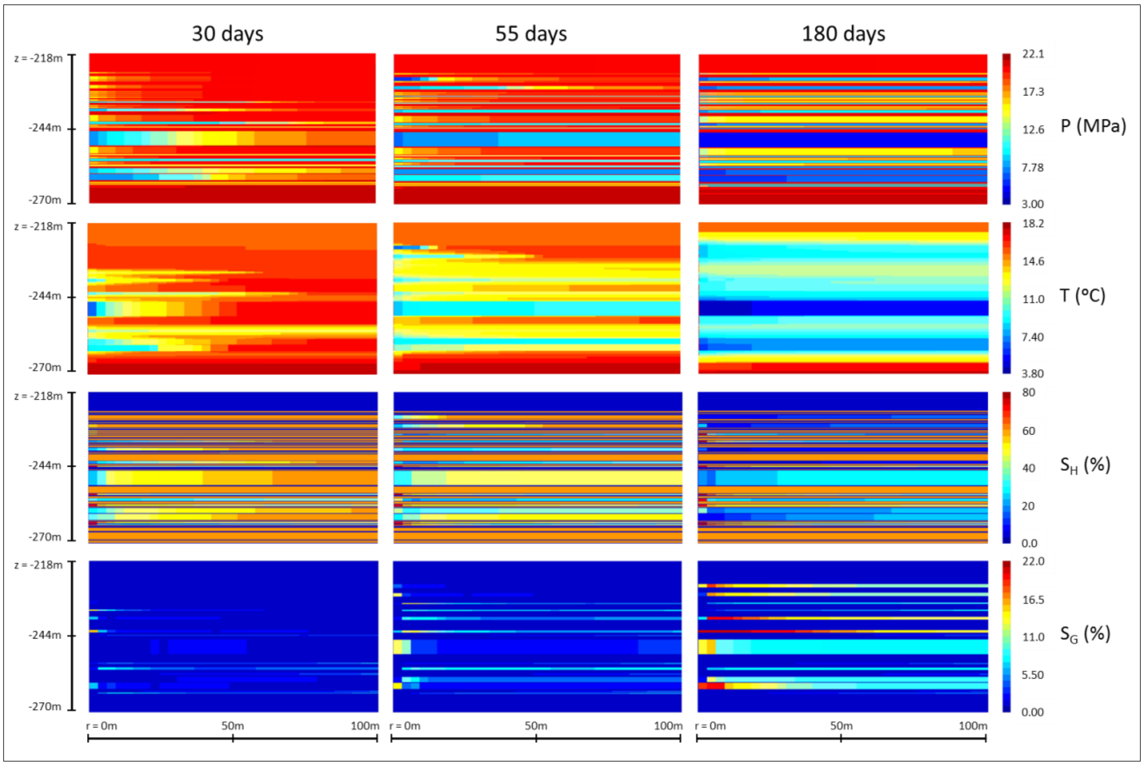

Fig. 7 – Spatial distribution of Pressure, Temperature, Hydrate Saturation and Gas Saturation for prospect HP11-A at three different times (30 days, 55 days and 180 days)

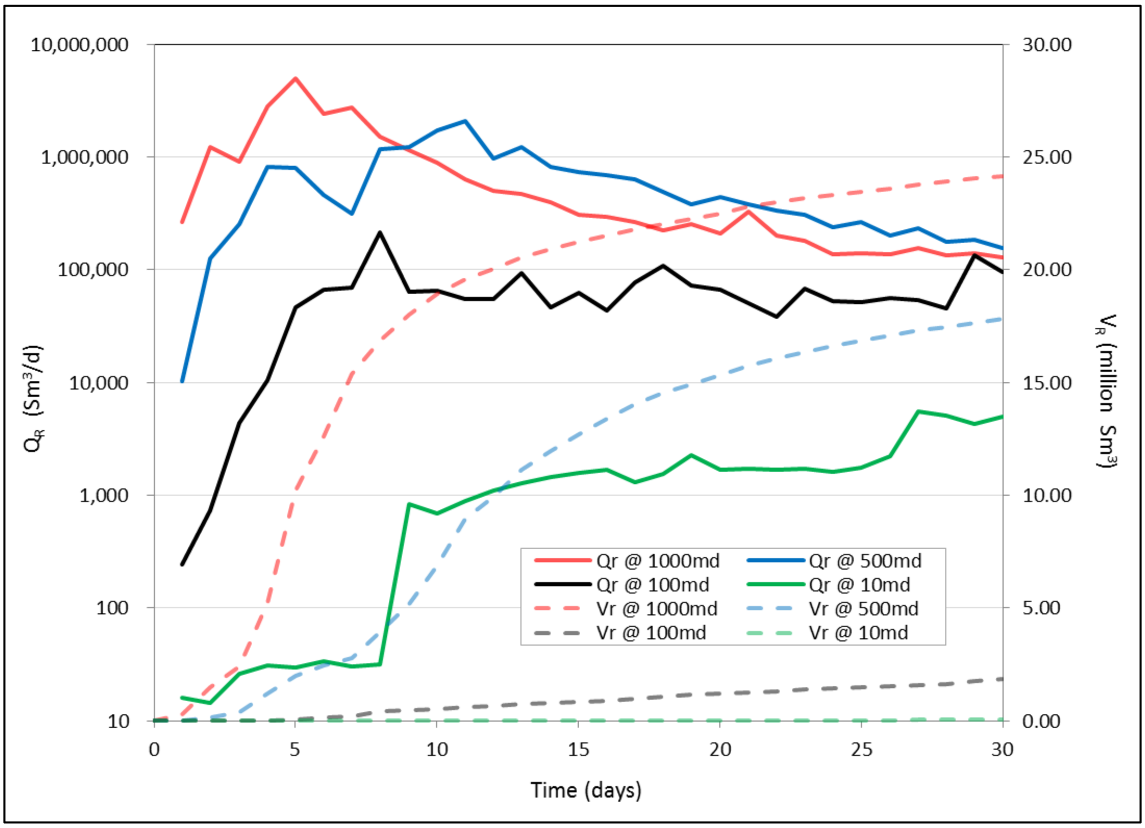

Fig. 8 – Sensitivity analysis to permeability showing gas release rate and cumulative gas volume from prospect HP11-A

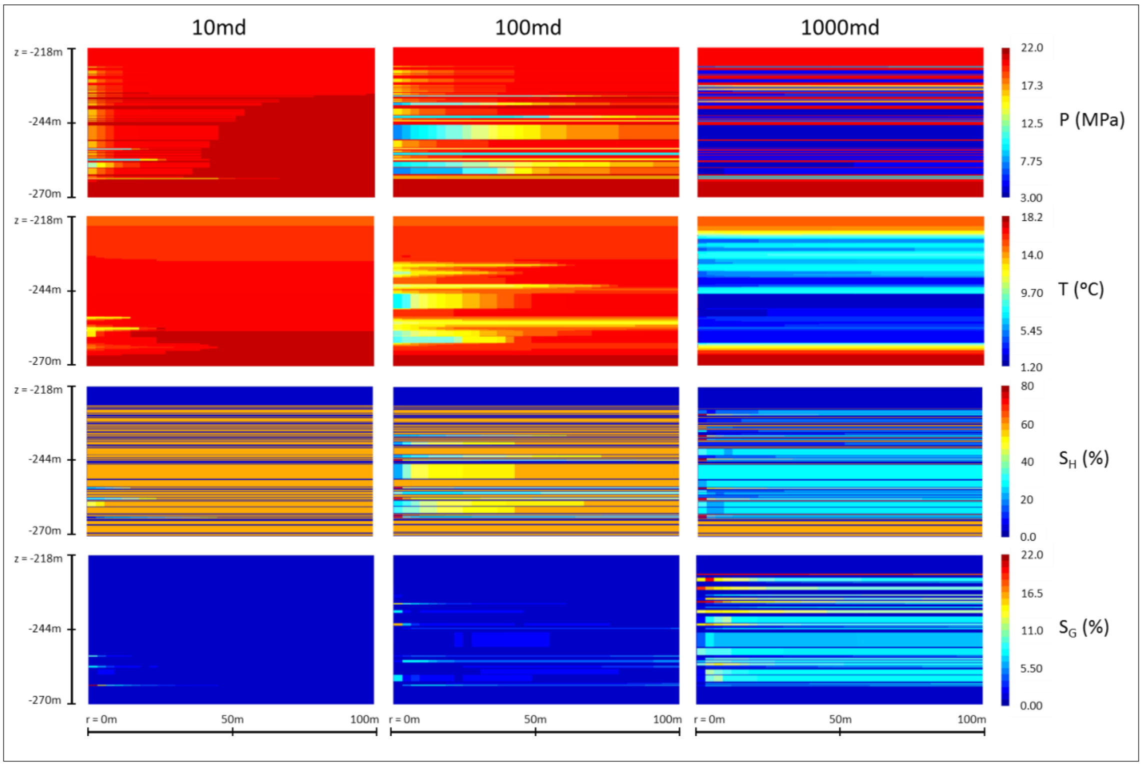

Fig. 9 – Spatial distribution of Pressure, Temperature, Hydrate Saturation and Gas Saturation for prospect HP11-A at 30 days for three permeability scenarios (10md, 100md and 1000md)

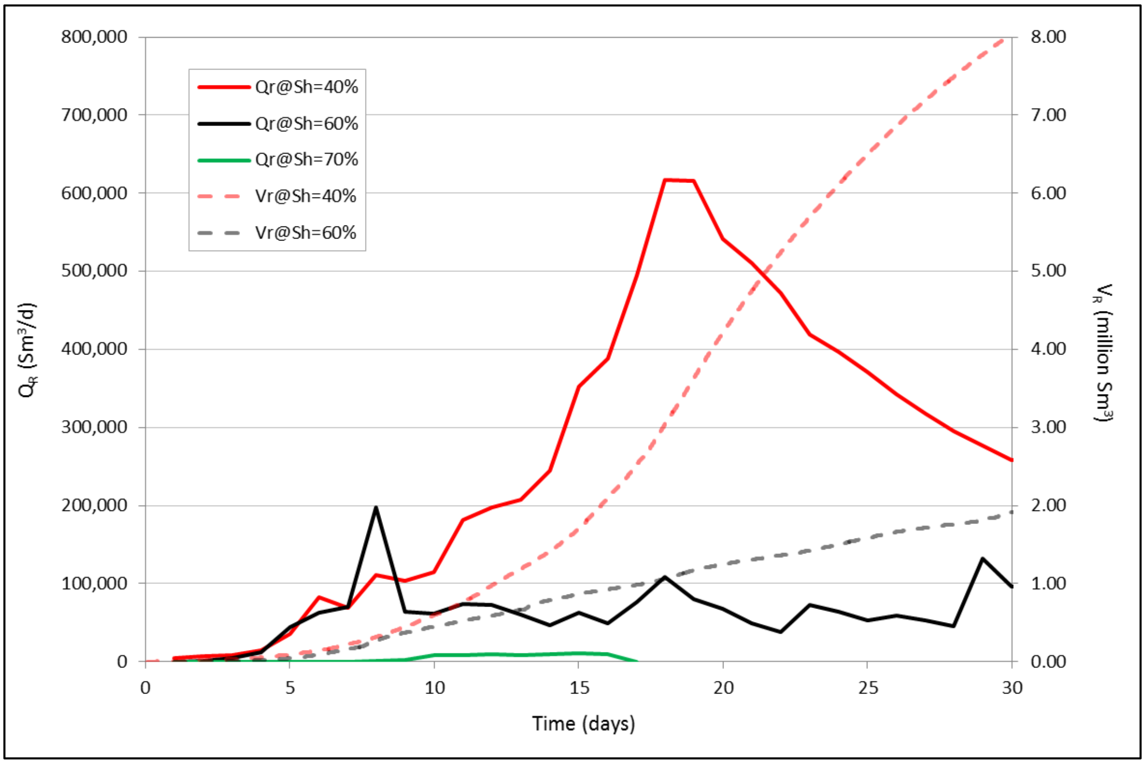

Fig. 10 – Sensitivity analysis to Hydrate Saturation for gas release rate and cumulative gas volume released from prospect HP11-A

Survey	Acquisition Company	Year	Coverage (Km^2)
YPF13	WesternGeco	2013	2,062
UR12	PGS	2012-2014	15,675
TO12	WesternGeco	2012-2014	7,166
BG12	Polarcus	2012-2014	13,545

Table 1 - 3D seismic surveys used for the identification of gas hydrate areas

Deposit type	Reservoir value
Turbidite	High
Channel fill	Medium-High
Shelf to Slope Progradations	Medium
Contouritic Terrace	Medium-Low
Contouritic Drift	Low
Mass Transport	Low

Table 2 - Criteria to assign expected reservoir quality to each type of deposits

Prospect	Thickness (m)	Expected Reservoir Quality
11-A	50	High
25	41	High
8-D	160	Medium-High
22-A	51	Medium-High
34-A	43	Medium-High
18-A	58	Low
35-A	51	Low
32-A	38	Low

Table 3 - Prospect ranking indicating approximate average gross thickness and expected reservoir quality.

9. REFERENCES

Anderson, Brian, Steve Hancock, Scott Wilson, Christopher Enger, Timothy Collett, Ray Boswell, and Robert Hunter. 2011. "Formation pressure testing at the Mount Elbert Gas Hydrate Stratigraphic Test Well, Alaska North Slope: Operational summary, history matching, and interpretations." *Marine and Petroleum Geology* 28 (2):478-492. doi: https://doi.org/10.1016/j.marpetgeo.2010.02.012.

Boswell, Ray, Timothy S. Collett, Evgeniy Myshakin, Taiwo Ajayi, and Yongkoo Seol. 2017. "The Increasingly Complex Challenge of Gas Hydrate Reservoir Simulation." 9th International Conference on Gas Hydrates (ICGH9), Denver, Colorado - USA.

Boswell, Ray, David Schoderbek, Timothy S. Collett, Satoshi Ohtsuki, Mark White, and Brian J. Anderson. 2016. "The Iġnik Sikumi Field Experiment, Alaska North Slope: Design, Operations, and Implications for CO2–CH4 Exchange in Gas Hydrate Reservoirs." *Energy & Fuels* 31 (1):140-153. doi: 10.1021/acs.energyfuels.6b01909.

Chong, Zheng Rong, She Hern Bryan Yang, Ponnivalavan Babu, Praveen Linga, and Xiao-Sen Li. 2016. "Review of natural gas hydrates as an energy resource: Prospects and challenges." *Applied Energy* 162:1633-1652. doi: https://doi.org/10.1016/j.apenergy.2014.12.061.

CMG. 2017. "CMG STARS Thermal & Advanced Processes Reservoir Simulator." ttp://www.cmgl.ca/stars/resource-library.

Dallimore, S.R., J.F. Wright, K. Yamamoto, and G. Bellefleur. 2012. Proof of concept for gas hydrate production using the depressurization technique, as established by the JOGMEC/NRCan/Aurora Mallik 2007-2008 Gas Hydrate Production Research Well Program. In *Scientific results from the JOGMEC/NRCan/Aurora Mallik 2007–2008 Gas Hydrate Production Research Well Program, Mackenzie Delta, Northwest Territories, Canada* Geological Survey of Canada, Bulletin 601.

De Santa Ana, H., N. Ucha, L. Gutiérrez, and G. Veroslavsky. 2004. Gas hydrates: Estimation of the gas potential from reflection seismic data in the continental shelf of Uruguay. Revista de la Sociedad Uruguaya de Geología.

Dillon, William P., and Michael D. Max. 2003. "Oceanic Gas Hydrate." In *Natural Gas Hydrate: In Oceanic and Permafrost Environments*, edited by Michael D. Max, 61-76. Dordrecht: Springer Netherlands.

DNE-MIEM. 2016. "Balance Energético Nacional (Preliminar)." http://www.dne.gub.uy/.

Freudenthal, T., and G. Wefer. 2013. "Drilling cores on the sea floor with the remote-controlled sea floor drilling rig MeBo." *Geoscientific Instrumentation* 2 (2):329-337. doi: 10.5194/gi-2-329-2013.

Fujii, Tetsuya, Kiyofumi Suzuki, Tokujiro Takayama, Machiko Tamaki, Yuhei Komatsu, Yoshihiro Konno, Jun Yoneda, Koji Yamamoto, and Jiro Nagao. 2015. "Geological setting and characterization of a methane hydrate reservoir distributed at the first offshore production test site on the Daini-Atsumi Knoll in the eastern Nankai Trough, Japan." *Marine and Petroleum Geology* 66:310-322. doi: 10.1016/j.marpetgeo.2015.02.037.

Gaddipati, Manohar, and Brian James Anderson. 2012. "3D Reservoir Modeling of Depressurization-Induced Gas Production from Gas Hydrate Reservoirs at the Walker Ridge Site, Northern Gulf of Mexico." Offshore Technology Conference, 2012/4/30/.

Giberto, D. A., C. S. Bremec, E. M. Acha, and H. Mianzan. 2004. "Large-scale spatial patterns of benthic assemblages in the SW Atlantic: the Río de la Plata estuary and adjacent shelf waters." *Estuarine, Coastal and Shelf Science* 61 (1):1-13. doi: 10.1016/j.ecss.2004.03.015.

Gray, Amanda. 2014. Seabed geomorphology and gas hydrate distribution, offshore Uruguay. In *MSc Thesis (unpublished)*. University of Aberdeen.

Hensen, Christian, Matthias Zabel, Kerstin Pfeifer, Tilmann Schwenk, Sabine Kasten, Natascha Riedinger, Horst D. Schulz, and Antje Boetius. 2003. "Control of sulfate pore-water profiles by sedimentary events and the significance of anaerobic oxidation of methane for the burial of sulfur in marine sediments." *Geochimica et Cosmochimica Acta* 67 (14):2631-2647. doi: 10.1016/S0016-7037(03)00199-6.

Hernández-Molina, F. Javier, Matías Soto, Alberto R. Piola, Juan Tomasini, Benedict Preu, Phil Thompson, Gianluca Badalini, Adam Creaser, Roberto A. Violante, Ethel Morales, Marcelo Paterlini, and Héctor De Santa Ana. 2016. "A contourite depositional system along the Uruguayan continental margin: Sedimentary, oceanographic and paleoceanographic implications." *Marine Geology* 378:333-349. doi: http://dx.doi.org/10.1016/j.margeo.2015.10.008.

IHS_Energy. 2017. International Energy Letter. In *China, Gas hydrate trial production successfully completed*.

Johnson, Arthur, and Michael Max. 2017. Technology Options to Enable Low Environmental Risk Production of Natural Gas Hydrate. 9th International Conference on Gas Hydrates, Denver Colorado, USA.

Kamath, V. A., and G. D. Holder. 1987. "Dissociation heat transfer characteristics of methane hydrates." *AIChE Journal* 33 (2):347-350. doi: 10.1002/aic.690330228.

Konno, Yoshihiro, Tetsuya Fujii, Akihiko Sato, Koya Akamine, Motoyoshi Naiki, Yoshihiro Masuda, Koji Yamamoto, and Jiro Nagao. 2017. "Key Findings of the World's First Offshore Methane Hydrate Production Test off the Coast of Japan: Toward Future Commercial Production." *Energy & Fuels* 31 (3):2607-2616. doi: 10.1021/acs.energyfuels.6b03143.

Konno, Yoshihiro, Jun Yoneda, Kosuke Egawa, Takuma Ito, Yusuke Jin, Masato Kida, Kiyofumi Suzuki, Tetsuya Fujii, and Jiro Nagao. 2015. "Permeability of sediment cores from methane hydrate deposit in the Eastern Nankai Trough." *Marine and Petroleum Geology* 66:487-495. doi: 10.1016/j.marpetgeo.2015.02.020.

Kowalsky, Michael B., and George J. Moridis. 2007. "Comparison of kinetic and equilibrium reaction models in simulating gas hydrate behavior in porous media." *Energy Conversion and Management* 48 (6):1850-1863. doi: https://doi.org/10.1016/j.enconman.2007.01.017.

Kurihara, M., A. Sato, H. Ouchi, H. Narita, T. Ebinuma, K. Suzuki, Y. Masuda, T. Saeki, K. Yamamoto, and T. Fujii. 2010. "Prediction of production test performances in Eastern Nankai trough methane hydrate reservoirs using 3D reservoir model." Proceedings of the Annual Offshore Technology Conference.

Kvenvolden, Keith A. 1988. "Methane hydrate — A major reservoir of carbon in the shallow geosphere?" *Chemical Geology* 71 (1):41-51. doi: https://doi.org/10.1016/0009-2541(88)90104-0.

Lavis, Owain, Mads Huuse, and Philip Thompson. 2017. "Integrated Overburden Fluid and Geothermal Characterization Offshore Uruguay." AAPG/SEG International Conference and Exhibition, London, England.

Makogon. 1997. *Hydrates of hydrocarbons / by Yuri F. Makogon*: PennWell.

Max, Michael D. 2006. *Economic Geology of Natural Gas Hydrate*. Edited by Arthur H. Johnson, William P. Dillon, SpringerLink, A. H. Johnson and Link, *Coastal Systems and Continental Margins*. Dordrecht: Dordrecht : Springer Netherlands.

Max, Michael D., and Arthur H. Johnson. 2016. *Exploration and Production of Oceanic Natural Gas Hydrate Critical Factors for Commercialization / by Michael D. Max, Arthur H. Johnson*. Edited by Arthur H. Johnson and SpringerLink, *Exploration and Production of Oceanic Natural Gas Hydrate*: Cham : Springer International Publishing : Imprint: Springer.

MH21. 2002. "MH21 Research Consortium." accessed 2017. http://www.mh21japan.gr.jp/english/mh21-2/1-2/.

Millero, Frank J., and Alain Poisson. 1981. "International one-atmosphere equation of state of seawater." *Deep Sea Research Part A. Oceanographic Research Papers* 28 (6):625-629. doi: http://dx.doi.org/10.1016/0198-0149(81)90122-9.

Morales, Ethel, Hung Kiang Chang, Matías Soto, Fernando Santos Corrêa, Gerardo Veroslavsky, Héctor de Santa Ana, Bruno Conti, and Gloria Daners. 2017. "Tectonic and stratigraphic evolution of the Punta del Este and Pelotas basins (offshore Uruguay)." *Petroleum Geoscience*. doi: 10.1144/petgeo2016-059.

Moridis, G. J. 2003. "Numerical Studies of Gas Production From Methane Hydrates." doi: 10.2118/87330-PA.

Moridis, G. J., Michael B. Kowalsky, and Karsten Pruess. 2012. TOUGH+HYDRATE v1.2 User's Manual: A Code for the Simulation of System Behavior in Hydrate-Bearing Geologic Media.

Moridis, G.J, and M.T. Reagan. 2007a. "Gas Production From Oceanic Class 2 Hydrate Accumulations." doi: 10.2118/0807-0069-JPT.

Moridis, George J., and Timothy S. Collet. 2003. "Strategies for Gas Production From Hydrate Accumulations Under Various Geological and Reservoir Conditions." Proceedings, TOUGH Symposium, Berkeley, California, USA.

Moridis, George J., Timothy S. Collett, Ray Boswell, Masanori Kurihara, Matthew T. Reagan, Carolyn Koh, and E. Dendy Sloan. 2009. "Toward Production From Gas Hydrates: Current Status, Assessment of Resources, and Simulation-Based Evaluation of Technology and Potential." doi: 10.2118/114163-PA.

Moridis, George J., Jihoon Kim, Matthew T. Reagan, and Se-Joon Kim. 2013. "Feasibility of gas production from a gas hydrate accumulation at the UBGH2-6 site of the Ulleung basin in the Korean East Sea." *Journal of Petroleum Science and Engineering* 108:180-210. doi: 10.1016/j.petrol.2013.03.002.

Moridis, George J., Michael B. Kowalsky, and Karsten Pruess. 2005. HydrateResSim User's Manual: A Numerical Simulator for Modelling the Behavior of Hydrates in Geologic Media. Berkeley, CA: Earth Sicences Division, Lawrence Berkeley National Laboratory.

Moridis, George J., and Matthew T. Reagan. 2007b. "Strategies for gas production from oceanic Class 3 hydrate accumulations."

Myshakin, Evgeniy M., Manohar Gaddipati, Kelly Rose, and Brian J. Anderson. 2012. "Numerical simulations of depressurization-induced gas production from gas hydrate reservoirs at the Walker Ridge 312 site, northern Gulf of Mexico." *Marine and Petroleum Geology* 34 (1). doi: 10.1016/j.marpetgeo.2011.09.001.

Myshakin, Evgeniy M., Jeen-Shang Lin, Shun Uchida, Yongkoo Seol, Timothy S. Collett, and Ray Boswell. 2017. Numerical Studies of Depressurization-Induced Gas Production from an Interbedded Marine Turbidite Gas Hydrate Reservoir Model. Proceedings of the 9th International Conference on Gas Hydrates.

Neben, S., B. Schreckenberger, J. Adam, and et al. 2005. Research Cuise BGR04, ARGURU—Geophysical Investigations Offshore Argentine and Uruguay with Akademik Alexandr Karpinsky. Buenos Aires-Buenos Aires, 19/11/ 2004 –

19/12/2004. Cruise Report and Preliminary Results Hannover, Germany: Bundesanstalt f¨ur Geowissenschaften und Rohstoffe.

NETL. 2017. "Hydrate Modeling - TOUGH+/HYDRATE & HIDRATERESSIM." https://www.netl.doe.gov/research/oil-and-gas/methane-hydrates/toughfx.

NOAA. 2013. WORLD OCEAN ATLAS 2013 version 2.

Schlitzer, R. 2014. Ocean Data View. In *http://odv.awi.de*.

Sloan. 1998. *Clathrate hydrates of natural gases / by E. Dendy Sloan*. 2nd ed. ed: Marcel Dekker.

Soto, Matías, Ethel Morales, Gerardo Veroslavsky, Héctor de Santa Ana, Nelson Ucha, and Pablo Rodríguez. 2011. "The continental margin of Uruguay: Crustal architecture and segmentation." *Marine and Petroleum Geology* 28 (9):1676-1689. doi: https://doi.org/10.1016/j.marpetgeo.2011.07.001.

Su, Zheng, George J. Moridis, Keni Zhang, Rui Yang, and Nengyou Wu. 2010. "SS - Gas Hydrate: Numerical Investigation of Gas Production Strategy for the Hydrate Deposits in the Shenhu Area." Offshore Technology Conference, 2010/1/1/.

Tomasini, Juan, Hector de Santa Ana, Bruno Conti, Santiago Ferro, Pablo Gristo, Josefina Marmisolle, Ethel Morales, Pablo Rodriguez, Matias Soto, and Gerardo Veroslavsky. 2011. "Assessment of Marine Gas Hydrates and Associated Free Gas Distribution Offshore Uruguay." *Journal of Geological Research* 2011:7. doi: 10.1155/2011/326250.

Uddin, M., Wright J.F., Dallimore S.R., and Coombe D. 2012. Gas hydrate production from the Mallik reservoir: numerical history matching and long-term production forecasting. In *Scientific results from the JOGMEC/NRCan/Aurora Mallik 2007-2008 gas hydrate production research well program, Mackenzie Delta, Northwest Territories, Canada* Geological Survey of Canada, Bulletin 601: Natural Resources Canada, Earth Sciences Sector, Geological Survey of Canada

Van Genuchten, M Th. 1980. "A closed-form equation for predicting the hydraulic conductivity of unsaturated soils." *Soil science society of America journal* 44 (5):892-898.

Wang, Yi, Jing-Chun Feng, Xiao-Sen Li, Yu Zhang, and Gang Li. 2016. "Evaluation of Gas Production from Marine Hydrate Deposits at the GMGS2-Site 8, Pearl River Mouth Basin, South China Sea." *Energies* 9 (3):222.

White, M.D., and M. Ostrom. 2006. STOMP Subsurface Transport Over Multiple Phase: User`s Guide PNNL-15782. edited by UNITED STATES DEPARTMENT OF ENERGY PACIFIC NORTHWEST NATIONAL LABORATORY.

Wilder, Joseph W., George J. Moridis, Scott J. Wilson, Masanori Kurihara, Mark D. White, Yoshihiro Masuda, Brian J. Anderson, Timothy S. Collet, Robert B. Hunter, Hideo Narita, Mehran Pooladi-Darvish, Kelly Rose, and Ray Boswell. 2008. "An International Effort to Compare Gas Hydrate Reservoir Simulators." Proceedings of the 6th International Conference on Gas Hydrates (ICGH 2008), Vancouver, British Columbia, CANADA.

Zhou, Mingliang, Kenichi Soga, Ermao Xu, Shun Uchida, and Koji Yamamoto. 2014. "Numerical Study on Eastern Nankai Trough gas Hydrate Production Test." Offshore Technology Conference, 2014/5/5/.

10. APPENDICES

Appendix A HydrateResSim simulator

Unless specifically stated, the following information on this section comes from HydrateResSim user´s manual (Moridis, Kowalsky, and Pruess 2005).

In addition to heat, the model can consider up to four mass components (water, methane, hydrate and inhibitors) within four possible phases (gas, liquid, ice and hydrate). The model presents the options for simulate the hydrate formation and dissociation with equilibrium or kinetic models.

Every possible hydrate dissociation process can be simulated with this code including depressurization, thermal stimulation and inhibition, individually and in co-stimulation.

The assumptions for the validity of the physical, thermodynamic and mathematical model are the following:

- Valid Darcy`s law for the system
- Mechanical dispersion is neglected compared with advection for the transport of dissolved gases and inhibitors
- Same compressibility and thermal expansivity between hydrate and ice
- The effects caused by different densities of liquid and ice phases on pressure are accommodated through a relatively high pore compressibility and the movement of the geologic medium while freezing is not described
- During water freezing, precipitation of dissolved salts do not occur as their concentration increases
- The thermophysical properties of the liquid phase are not affected by the dissolved inhibitors
- The pressure is lower than 6800 psi (46.9 MPa).

Details about the underlying physics and governing equations for this simulator are presented on the user´s manual (Moridis, Kowalsky, and Pruess 2005). Main concepts are outlined below:

The amount of CH_4-Hydrate formed or CH_4 gas released is defined from the following reaction:

$$CH_4(gas) + N_H H_2O(water\ or\ ice) = CH_4 \cdot N_H H_2O\ (solid)$$

Being N_H the hydration number for methane (HydrateResSim can only model the behavior of methane hydrates).

The already mentioned four components (hydrate, water, methane and inhibitor), with the inclusion of heat are considered in mass and heat balance equations for every grid-block. Mass and heat accumulation terms are considered as well as flux and source/sink terms both for equilibrium and kinetic case.

HydrateResSim includes thermophysical properties for water, CH_4-Hydrate and CH_4-Gas as well as hydrate phase relationships. Additionally the effect of inhibitor on hydrate equilibrium is also taken into account.

The effect of solid phases (hydrate and/or ice) in the flow through the porous media is described by the concept of original porous medium. This model considers that porosity and absolute permeability are not affected by the appearance of solid phases (however porosity can change due to variations in temperature and pressure). In this concept, relative permeabilities are controlled by different phase saturations (i.e. gas phase relative permeability depends only on gas saturation, and is the same regardless of how much of the fraction (1-Sg) of the pore space is shared between liquid and solid phases).

The simulator presents the option to apply permeability modification coefficients for individual grid blocks to affect the absolute permeability of each grid block.

Regarding the geological media, the following represents the input parameters: Material name; Rock grain density; Default porosity; Absolute permeabilities on x, y and z directions; Heat conductivity of the formation (at S_w=1); Specific heat of rock grain; Radius of rock grain (only for the kinetic model option); Pore compressibility; Pore thermal expansivity; Heat conductivity of the formation (desaturated); Tortuosity factor for binary diffusion; Klinkenberg "b" parameter; Relative permeabilities function option and parameters; Capillary pressure function option and parameters.

HydrateResSim code has the option also to describe flow in fractured media by double-porosity model.

Considering the all the possible components and phase combinations, a total of 11 states are described by the simulator for the equilibrium hydration reaction option as presented in the following table.

Phase	State Identifier	Primary Variable 1	Primary Variable 2	Primary Variable 3
1-Phase: G	Gas	P_gas	Y_m_G	T
1-Phase: A	Aqu	P	X_m_A	T
2-Phase: A+G	AqG	P_gas	S_aqu	T
2-Phase I+G	IcG	P_gas	S_ice	T
2-Phase A+G	AqH	P	S_aqu	T
2-Phase: I+H	IcH	P	S_ice	T
3-Phase: A+H+G	AGH	S_gas	S_aqu	T
3-Phase:A+I+G	AIG	P_gas	S_aqu	S_gas
3-Phase: A+I+H	AIH	P	S_aqu	S_ice
3-Phase: I+H+G	IGH	S_gas	S_ice	T
Quadruple Point: I+H+A+G	QuP	S_Gas	S_aqu	S_ice

Table A-1 The possible primary variables are: P = Pressure (Pa); P_gas = gas pressure (Pa); T = Temperature (ºC); X_m_A = mass fraction of CH4 dissolved in the aqueous phase; Y_m_G = mass fraction of CH4 dissolved in the gas phase; S_aqu = liquid saturation; S_gas = gas saturation; S_ice = ice saturation. From (Moridis, Kowalsky, and Pruess 2005)

These primary variables are necessary and sufficient to uniquely define the system.

Equations are discretized in space by the integral finite difference method while time is discretized as a first-order finite difference, solving the equations by Newton/Raphson iteration method.

HydrateResSim allows the use of Dirichlet (thermodynamic conditions i.e. P, T) or Neumann type boundary conditions (fluxes of mass or heat across boundary surfaces). By default, the Neumann boundary condition of no flux is present. Introducing sink or sources into elements adjacent to boundary, general flux conditions can be stablished. On the other hand, Dirichlet conditions can be imposed by assigning very large volumes to grid blocks adjacent to the boundary. For time-independent Dirichlet boundary conditions, the model allows the definition of inactive elements (their thermodynamic conditions remain unchanged during the simulation).

The simulator present the possibility of define several computation parameters as well as an optional block to specify parameters used by linear equation solvers.

Appendix B Validation of the simulator

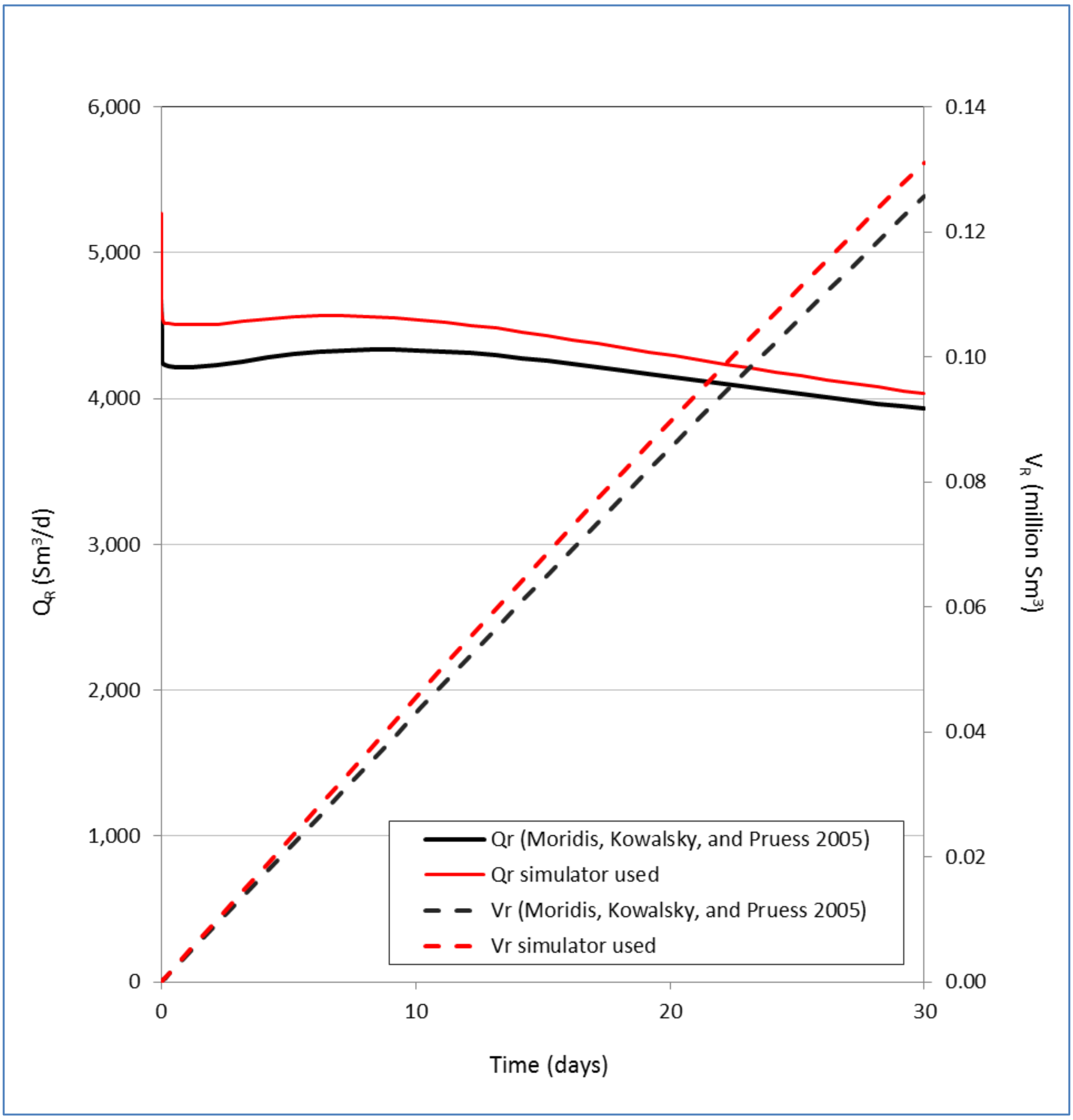

Fig. B – 1 Comparison of results for gas release rate and cumulative gas release volume between available simulator and values presented in (Moridis, Kowalsky, and Pruess 2005).

Appendix C Model parameters from selected references

	Reference	Su et al 2010	Kurihara et al 2010	Kurihara et al 2010	Gaddipati and Anderson 2012	Myshakin et al 2012	Myshakin et al 2012	Moridis et al 2013	Zhou et al 2014	Konno et al 2017	Myshakin et al 2017
General Information	**Country**	China	Japan	Japan	USA	USA	USA	Korea	Japan	Japan	Not specified
	Location	South China Sea / Shenhu area	eastern Nankai Trough	eastern Nankai Trough	Walker Ridge, Northern Gulf of Mexico	Walker Ridge, Northern Gulf of Mexico	Walker Ridge, Northern Gulf of Mexico	Ulleung basin	eastern Nankai Trough	eastern Nankai Trough	Not specified
	Prospect / Site	SH2	α	β	WR 313G	WR 313G	WR 313H	UBGH2-6	not specified	AT1 (β)	Not specified
	Simulator	Serial and parallel TOUGH+HYDRATE	MH21-HYDRES	MH21-HYDRES	CMG STARS	parallell version of TOUGH+HYDRATE	parallell version of TOUGH+HYDRATE	Serial and parallel versions of the TOUGH+HYDRATE coupled with the FLAC3D geomechanical model	CMHGS	MH21-HYDRES	parallel version of TOUGH+HYDRATE
	Water depth (m)	1235	720 (from figure)	1000 (from figure)	2000m estimated	not specified	not specified	2160	1000	1000	2575
	Top of reservoir unit (mbsf)	188	93.8	268.1	870	830	830	140	260	278	272.8
	base of GHSZ (mbsf)	228	200.3	338.6	940	not specified	not specified	175	not specified	300	290.6
	Gross Thickness of interest unit (m)	40	106.5	50.4	70	48.8	61	20	70	60	24.1
	Subunits thickness / discretization (m)	0.25	0.4 m or less	not specified	not specified	variable 0.6 to 2 m	variable 0.3 to 9 m	0.1	minimum of 4 m in the production zone	variable (tens of centimeters to few meters)	0.1
	Number of subunits (layers)	160	not specified	not specified	37	3D: 27; 2D: 200	3D: 45; 2D: 100	200	not specified	not specified	241
Productive unit	**Sand porosity (%)**	38	variable 25 to 45	variable 35 to 40	40% (average)	variable	variable	variable 52 to 70	not specified	variable from 30 to 50	40
	Hydrate saturation at sand (%)	40	variable, up to 80	variable, up to 80	variable up to 90	variable	variable	variable 30 to 70	not specified	variable, up to 80	80
	Irreducible water saturation at sand (%)	30	27	27	20	18	18	20	not specified	not specified	10
	Intrinsic permeability at sand (mD)	10	1000	1000	1000mD horizontal, 100mD vertical	1000mD horizontal, 100mD vertical	1000mD horizontal, 100mD vertical	500	not specified	variable, exceeding 1000	1000
	Effective permeability at sand with hydrate(mD)	not specified	not specified	not specified	not specified	not specified	not specified	not specified	not specified	variable from 1 to 10	0.1 or 10
	Effective permeability at sand with water(mD)	not specified	not specified	not specified	not specified	not specified	not specified	not specified	not specified	variable, exceeding 1000	1000
	Thermal conductivity of sand porous media dry/wet (W/mK)	1/3.1	2.915 (for sand and silt layers)	2.915 (for sand and silt layers)	not specified	not specified	not specified	1 /1.45	not specified	not specified	0.37 / 2.28

Productive unit	**mud porosity (%)**	not specified	variable	variable	1	different cases tested for the under/overburden: 1%, 10%	different cases tested for the under/overburden: 1%, 10%	variable 45 to 55	not specified	variable	40
	hydrate saturation at mud (%)	not specified	0	0	0	0	0	0	0	0	0
	Bound water saturation at mud (%)	not specified	not specified	not specified	not specified	not specified	not specified	0.5	not specified	not specified	90
	intrinsic permeability at mud (mD)	10	100 mD for silt and 10 mD for mud layers	100 mD for silt and 10 mD for mud layers	0.01mD horizontal, 0.001 mD vertical	3D: different cases tested for the under/overburden: 0.1/0.01mD and 1/0.1mD (horizontal/vertical) 2D: 0/0mD and 0.01-10mD	3D: different cases tested for the under/overburden: 0.1/0.01mD and 1/0.1mD (horizontal/vertical) 2D: 0/0mD and 0.01-10mD	0.55 mD (clay interlayers)	not specified	0.01 (clayey silt layers)	0.0005
	Thermal conductivity of mud porous media dry/wet (W/mK)	1/3.1	1.7	1.7	2.0 W/mK Dry	1/3.1	1/3.1	1 /1.45	not specified	not specified	0.36 / 1.95
	Pore compressibility (Pa-1)	not specified	not specified	not specified	1.00E-09	1.00E-09	1.00E-09	not specified	not specified	not specified	1.20E-08
	Rock density (kg/m3)	2600	not specified	not specified	2600	2600	2600	2750 (mud), 2650 (sand)	2040 (saturated bulk density)	not specified	2750
	Rock grain specific heat (J/kg ºC)	not specified	not specified	not specified	1000	1000	1000	not specified	not specified	not specified	1000
	Relative pemeability model	presenting equations and parameters (SirG=0.03; SirA=0.3)	"expressed as cubic polinomial (irreducible water saturation: 27%, critical gas saturation: 3%)..."	"expressed as cubic polinomial (irreducible water saturation: 27%, critical gas saturation: 3%)..."	modified Stone three-phase model	modified Stone three-phase model (parameters from Anderson et al 2011)	modified Stone three-phase model (parameters from Anderson et al 2011)	EPM - (Moridis et al 2008) presenting parameters	(Van Genuchten 1980) presenting calibrated curves and parameters	Not specified	(Brooks and Corey 1964)
	Capilary pressure model	(Van Genuchten 1980) presenting parameters	not specified	not specified	(Van Genuchten 1980) presenting parameters	(Van Genuchten 1980) presenting parameters from Anderson et al 2011	(Van Genuchten 1980) presenting parameters from Anderson et al 2011	(Van Genuchten 1980) presenting parameters	(Uchida 2012)	Not specified	(Van Genuchten 1980) and parameters from (Anderson et al 2011)
	Porous media model	OPM	not specified	not specified	not specified	not specified	not specified	EPM	not specified	Not specified	OPM
Unit underneath	**Fluid content below base of GHSZ**	water	water	water	gas / water	water	water	water	water	water	water
	Thickness (m)	20	144	144	50	3D: 16m; 2D: 70m	3D: 30m; 2D: 70m	80	last unit is the interest unit	20	200 (arbitrary)
	Subunits thickness (m)	not specified	not specified	not specified	not specified	3D: 1.5 - 15m; 2D: logarithmically variable	3D: 30m; 2D: logarithmically variable	variable	-	variable	variable (0.5 - 5 -30)
	Number of subunits	not specified	not specified	not specified	not specified	3D: 2; 2D: 10	3D: 1; 2D:10	10 (from figure)	-	not specified	24

Geometry	**Modelled geometry**	Cylindrical	3D corner point grid	3D corner point grid	non-orthogonal 3D corner point grid	non-orthogonal 3D corner point grid and also 2D cylindrical model	non-orthogonal 3D corner point grid and also 2D cylindrical model	Cylindrical	Two cases, cylindrical and plane-strain tilted 10deg	Cylindrical	Cylindrical
	rw (m)	0.1	not specified	not specified	not specified	0.111	0.111	0.1	0.15	0.108	0.15
	Total vertical distance simulated (m)	80	344.3	700	not specified	3D model:91	3D model: 194	220	380	100.25	496.9
	Total number of layers	242	747	444	not specified	3D model: 35; 2D model: 222	3D model: 65; 2D model: 222	240	38	202	404
	Lateral distance extension from well (m)	100	500 to 550	500	min aprox 450m	two cases for 2D: 450m and 1500m	two cases for 2D: 450m and 1500m	250	300	5000	500
	number gridblocks from well (radial)	105	-	-	not specified	two cases for 2D: 80 and 100	two cases for 2D: 80 and 100	160	23 and 46	120	100
	Grid lengh distribution type	not specified	-	-	not specified	logarithmic	logarithmic	logarithmic	not specified	logarithmic	logarithmic
	number of grid blocks	25410	7208710	3234540	not specified	2D: 18204 and 22644	2D: 10004 and 12444	38400	874 and 1748	not specified	35905
	number of connections	not specified	not specified	not specified	not specified	2D: 36104 and 44964	2D: 19804 and 24664	not specified	not specified	not specified	71354
Boundary conditions	**Lateral**	not specified	not specified	not specified	not specified	No heat and no flux	No heat and no flux		not specified	not specified	No mass or heat flow
	Top	constant T	not specified	not specified	not specified	Fixed	Fixed	constant-flow with constant conditions and properties	not specified	not specified	Fixed
	Bottom	constant T	not specified	not specified	not specified	Fixed	Fixed	constant-flow with constant conditions and properties	not specified	not specified	Fixed

Initial conditions	**Pore pressure distribution**	hydrostatic (ocean water density at atmospheric pressure = 1035kg/m3)	hydrostatic	hydrostatic	not specified	hydrostatic	hydrostatic	hydrostatic	not specified	graph included	hydrostatic
	Geothermal gradient (ºC/mbsf)	0.047	0.03	0.03	0.0196	not specified	0.0196	0.0864	0.03	graph included	0.0663
	Seafloor temperature (ºC)	not specified	not specified	not specified	not specified	not specified	not specified	not specified	3.75	not specified	1.9855
	Pore water salinity (ppm)	30000	35000	35000	not specified	35000	35000	not specified	35000	not specified	35000
	Effect of salt on equilibrium P/T	not specified	not specified	not specified	not specified	Dickens et al 1997	Dickens et al 1997	not specified	Calibrated to Peq = exp (39.10 - 8508/T)	not specified	Dickens et al 1997
	Peq at Base of GHSZ (MPa)	14.97	not specified	not specified	not specified	not specified	not specified	not specified	not specified	graph included	28.73
	Teq at Base of GHSZ (ºC)	14.87	not specified	not specified	not specified	not specified	not specified	not specified	not specified	graph included	19.89
	equilibrium initialization procedure	Moridis and Kowaldky 2006, Moridis and Reagan 2007, Moridis et al 2007	not specified	not specified	not specified	similar to Moridis et al 2005	similar to Moridis et al 2005	Moridis and Reagan 2007a, 2007b	not specified	not specified	similar to Moridis et al 2005
	Temperature range at hydrate bearing interval (ºC)	not specified	not specified	not specified	not specified	not specified	not specified	6.366-25.48	not specified	graph included	19-20
Modelled well	**Geomechanical considerations**	No	No	No	not specified	not specified	not specified	Yes	Yes	No	No
	Completion lenght (m)	14	99.6	36.2	not specified	not specified	not specified	not specified	50	38	17 and 17.8
	Constant pressure (MPa)	3	3	3	2.7	2.7	2.7	3	different scenarios of pressure reduction to reach 3MPa	5MPa four days and 4.3MPa two days. Target pressure = 3MPa	3
	Constant pressure applied to	not specified	not specified	not specified	not specified	not specified	not specified	gridblock above the uppermost cell in the well (with null thermal conductivity and realistic temperature)	not specified	not specified	topmost grid block of the wellbore sub-domain
	Wellbore sub-domain	pseudo-porous medium (1000-10000 D axial and 1-10D radial; Pc=0, relative permeability was a linear function o the phase saturations in the wellbore, SirG=0.005)	not specified	not specified	not specified	Pseudoporous - medium aproach (Moridis and Reagan 2007)	Pseudoporous - medium aproach (Moridis and Reagan 2007)	pseudoporous-medium (5000 D and Pc=0 with linear relative permeability function of the phase saturation and irreducible gas saturation Sirg=0.005)	not specified	not specified	pseudoporous-medium approach (Moridis and Reagan 2007)

Appendix D Sequence of lithofacies for selected prospects

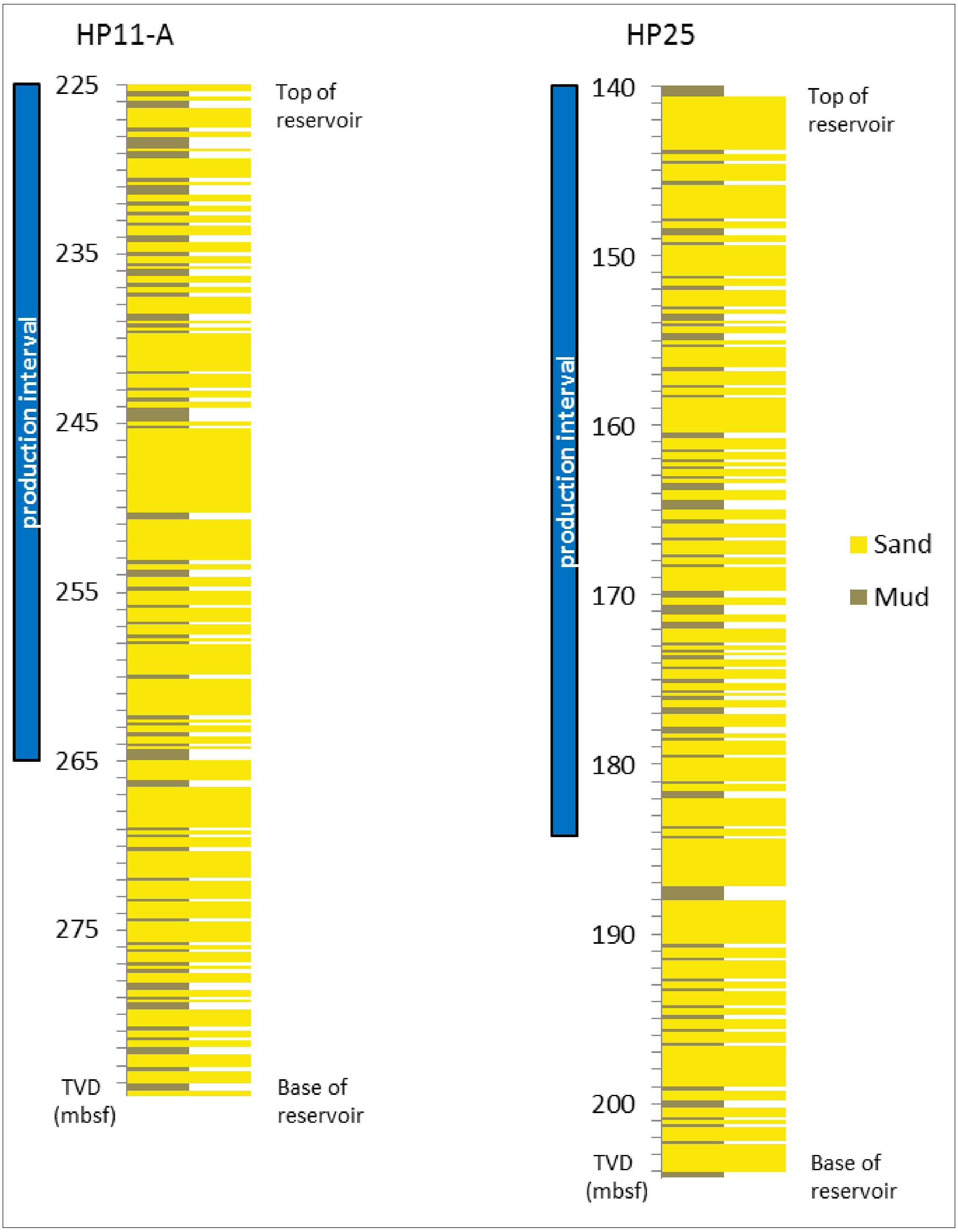

Fig. D-1 lithofacies distribution for each studied prospect

Appendix E Code Modifications regarding Relative Permeability Function

```
! ......... Aqueous phase relative permeability
! original HRS code:
!            IF(SS > 0.0d0) THEN
!              REPL = SQRT(SS)
!      &              *( 1.0d0 -( 1.0d0 - SS**( 1.0d0/xpn ))**xpn )**2
!            ELSE
!               REPL = 0.0d0
!            END IF
!
! modified with updated parameters from (Zhou et al 2014):
           IF(SS > 0.0d0) THEN
              REPL = ((SS)**6.2d-1)
     &              *( 1.0d0 -( 1.0d0 - SS**( 1.0d0/xpn ))**xpn )**2
           ELSE
              REPL = 0.0d0
           END IF
```

```
! original HRS code: ........... From the Corey [1954] model; non-zero irreducible gas saturation
!
!                   IF(SG <= Sg_irr) THEN
!                     REPG = 0.0d0
!                   ELSE
!                      SS = MIN(  1.0d0,
!     &                           MAX(    0.0d0,
!     &                                 ( (SL - Sw_irr)
!     &                                  /(1.0d0 - Sw_irr - Sg_irr)
!     &                                 )
!     &                              )
!     &                        )
!                      REPG = (1.0d0-SS)*(1.0d0-SS)*(1.0d0-SS*SS)
!                   END IF
!
!modified with updated parameters from (Zhou et al 2014)
                  IF(SG <= Sg_irr) THEN
                     REPG = 0.0d0
                  ELSE
                  REPG = ((1.0d0 - SS)**1.8d0)
     &                  *( ( 1.0d0 - SS**( 1.0d0/xpn ))**xpn )**2
                  END IF
!
```

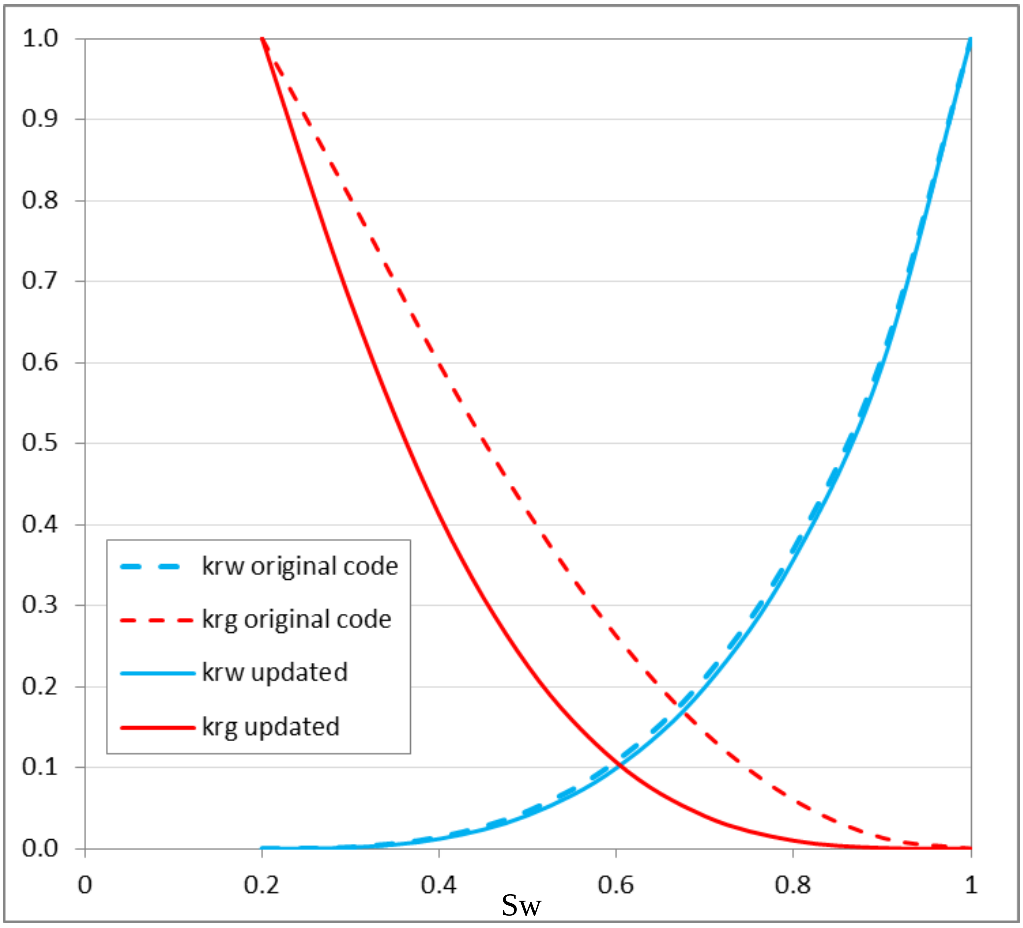

Fig. C-1 Original and updated relative permeability curves

Appendix F Code modifications regarding Capillary Pressure function

```
        CASE (1,8)
!
          m_inv =  1.0d0/(1.0d0-1.0d0/media(nmat)%ParCP(2))
          n_inv =  1.0d0/media(nmat)%ParCP(2)
          ! original HRS code:
          ! Pc_00 = -DW*9.806d0/media(nmat)%ParCP(3)
          ! modified code:
          Pc_00 = -media(nmat)%ParCP(3)
!
```

Input parameter 1 = S_{wir}

Input parameter 2 = n = 1 / (1- λ)

Input parameter 3 = Po.

Appendix G Code modifications regarding Hydrate Equilibrium Curves

```
!            Original HRS code
!               EqTemp_HydrCH4 = 8.5338d3/(3.898d1-P_x) - T_dev     ! in K
!
!            Updated according to Zhout et al 2014
                EqTemp_HydrCH4 = 8.508d3/(3.910d1-P_x) - T_dev     ! in K
!
```

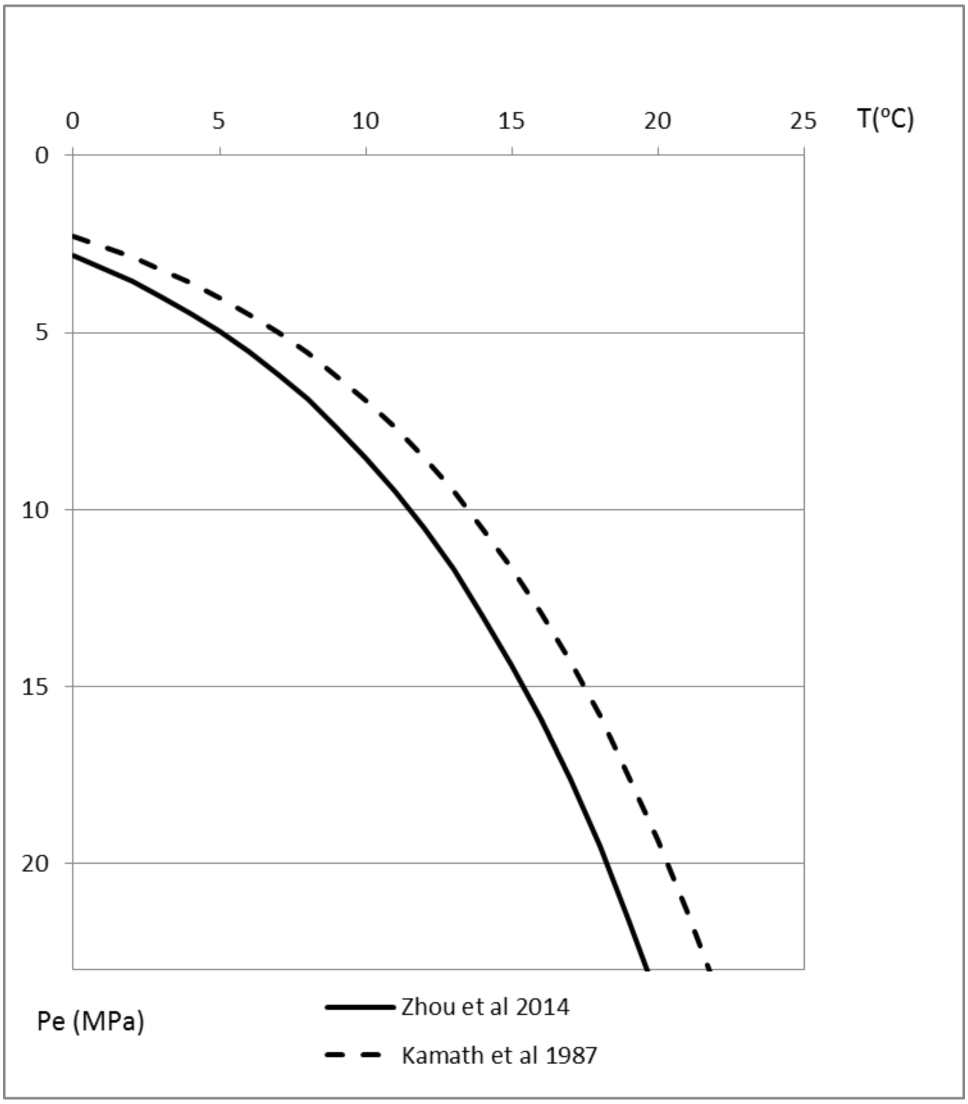

Fig. E-1 Effect of salinity (35,000ppm) on P-T equilibrium curve

Appendix H Seawater Temperature

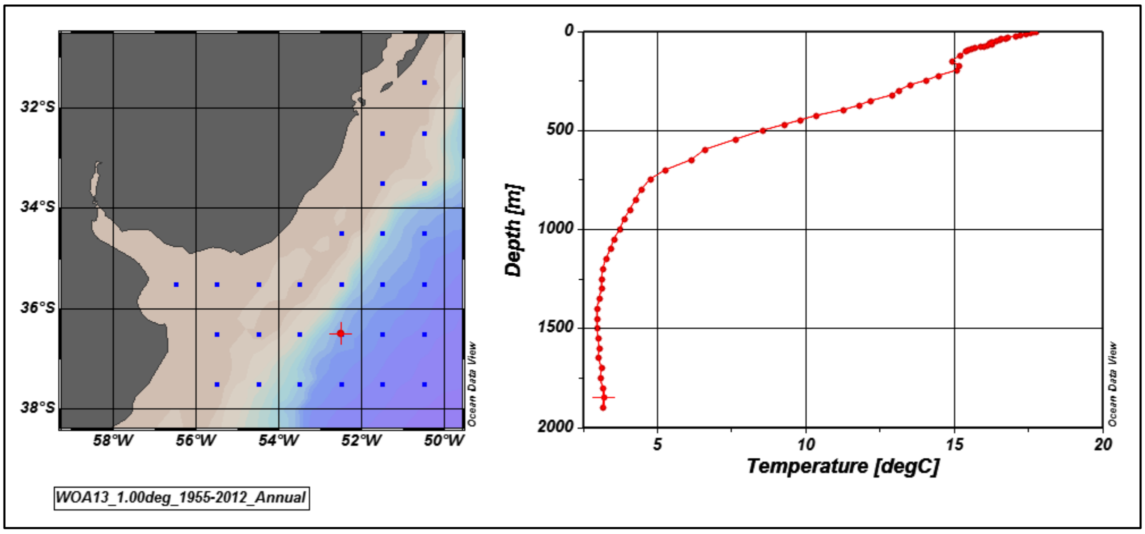

Fig. F-1 Seawater temperature from World Ocean Atlas Database (NOAA 2013) and Ocean Data View (Schlitzer 2014). Red cross in map at the left hand side and data at right hand side corresponds to Station 12301 (B)

Appendix I Summary of simulation model parameters

Parameter	value	
	HP11-A	HP25
Water depth	1850m	787.5m
Overburden thickness (above completion)	5m	5m
Underburden thickness (below completion)	5m	5m
Top of reservoir unit	225mbsf	140.5mbsf
base of GHSZ	285mbsf	204.4mbsf
Gross thickness of interest unit	60	64.4m
Layer thicknesses	As in Fig. 4	
Completion interval	225 - 265 mbsf	140.5 - 184.4 mbsf
borehole radius	0.15m	0.15m
Constant bottomhole pressure	3MPa	3MPa
Porosity	0.4	0.4
Initial S_H in hydrate-bearing sands	0.6	0.6
Initial T range at completion interval	15.7 - 17.8 °C	9.4 – 10.8 °C
Initial P range at completion interval	21.1 – 21.5 MPa	9.4 – 9.8 MPa
Gas composition	100% CH_4	100% CH_4
Water Salinity	35,000ppm	35,000ppm
Intrinsic horizontal permeability of sand	100md	100md
Intrinsic vertical permeability of sand	10md	10md
Intrinsic permeability of mud	0md	0md
Grain density (mud)	2,750 kg/m^3	2,750 kg/m^3
Grain density (sand)	2,650 kg/m^3	2,650 kg/m^3
Dry thermal conductivity	1 W/(mK)	1 W/(mK)
Wet thermal conductivity	3.1 W/(mK)	3.1 W/(mK)
Pore compressibility	1x10^{-9} Pa^{-1}	1x10^{-9} Pa^{-1}
Rock grain specific heat	1,000 J/kg°C	1,000 J/kg°C
Capillary pressure model (Van Genuchten 1980)	$P_{cap} = -P_o\left(S_e{}^{-1/\lambda} - 1\right)^{1-\lambda}$ $S_e = \dfrac{S_w - S_{wir}}{S_{w\_max} - S_{wir}}$	
$S_{w\ max}$	1	1
S_{wir}	0.19	0.19
λ	0.45 (sand); 0.15 (mud)	0.45 (sand); 0.15 (mud)
P_o	1x10^{4}Pa (sand); 1x10^5 Pa(mud)	1x10^{4}Pa (sand); 1x10^5 Pa(mud))
Relative permeability model (Van Genuchten 1980)	$k_{rw} = S_e{}^{b}\left[1-\left(1-S_e{}^{\frac{1}{\lambda}}\right)^{\lambda}\right]^2$ $k_{rg} = (1-S_e)^c\left(1-S_e{}^{\frac{1}{\lambda}}\right)^{2\lambda}$	
S_{wir}	0.2	0.2
S_{gir}	0.012	0.012
λ	0.85	0.85
b	0.62	0.62
c	1.8	1.8

Appendix J Details of Hydrate Accumulations identified

Acumulation	Water depth (m)	BSR depth (mbsf)	Geological interpretation	Comments	Interval of interest identified	Average thickness of interest interval (m)	Thickness in m of the interpreted deposit types within the interval of interest or GHSZ						Expected reservoir quality
							Turbidite	Channel fill	Shelf to Slope Progradations	Contouritic Terrace	Contouritic Drift	Mass Transport	
1	1396	176	Contourite (Plastered Drift D1)	Layered system with no observable channels within GHSZ, but possible channels at the free-gas zone	NO						176		
2	1560	272	stacked submarine channel system overlayed by contourite (Plastered Drift D1)	Most of the GHSZ at the Contourite drift but, BSR crosscutting channel system	NO			5			267		
3	1272	226	submarine channel and contourite (Plastered Drift D1)	Most of the GHSZ at the Contourite drift but, BSR crosscutting channel system, not very good seismic definition	NO			113			113		
4	1557	242	Sctacked submarine channel complex and contourite (Plastered Drift D1)	Most of the GHSZ at the Contourite drift but, BSR crosscutting channel system, not very good seismic definition	NO			81			161		
5	1917	206	Submarine channel below an active channel	Small area. Localized BSR restricted to the channel. Parallel reflectors, possibly fine sediments.	NO			206					
6	700	100	Smooth slope erosional surface	Limit of GHSZ at shallow waters (BSR pinching out the seafloor). Proximate to the Terrace and shelf. Progradations with posible sandy sediments. (also blanking at GHSZ)	NO				100				

Acumulation	Water depth (m)	BSR depth (mbsf)	Geological interpretation	Comments	Interval of interest identified	Average thickness of interest interval (m)	Thickness in m of the interpreted deposit types within the interval of interest or GHSZ						Expected reservoir quality
							Turbidite	Channel fill	Shelf to Slope Progradations	Contouritic Terrace	Contouritic Drift	Mass Transport	
7	1097	213	Submarine channel complex	Upper section of channel fill	NO			213					
8-A	1287	222	Contouritic terrace T2 (Ewing terrace) and paleocanyons	HAR indicative of possible sandy deposits (Hernández Molina et al 2016)	NO			89		133			
8-B	1480	286	Contourite (Plastered Drift D1) and some channels below the BSR		NO						286		
8-C	1914	363	Submarine channel and possible mass transport deposit above	Most of the channel fill outside the GHSZ	NO			121			121	121	
8-D	**2550**	**479**	Channel system above MTD	strong blanking at the GHSZ suggesting the presence of gas hydrates	**YES**	**160**		**160**					**Medium-High**
8-E	2789	474	MTC with some channel systems	Mostly chaothic reflectors, possibly low reservoir quality	NO							474	
9	1590	280	Plastered Drift D1		NO						280		
10	995	169	Upper slope progradation		NO				169				

Acumulation	Water depth (m)	BSR depth (mbsf)	Geological interpretation	Comments	Interval of interest identified	Average thickness of interest interval (m)	Thickness in m of the interpreted deposit types within the interval of interest or GHSZ						Expected reservoir quality
							Turbidite	Channel fill	Shelf to Slope Progradations	Contouritic Terrace	Contouritic Drift	Mass Transport	
11-A	**1954**	**294**	Posibly turbidite. Differential compaction? Plastered drift D2 on top. Abrupt termination of the body possibly due to erosion	Completely different seismic character regarding the soroundings (drifts) presenting blanking, possibly associated to high gas hydrate saturations. BSR crosscut the body on lanward direction. Possible class 1 prospect.	**YES**	**50**	**50**						**High**
12	900	160	Smooth slope erosional surface	Limit of GHSZ at shallow waters (BSR pinching out the seafloor)	NO				160				
13	2553	512	MTC with some channel systems	very chaotic sedimentary patterns, probably low reservoir properties	NO							512	
14	2827	528	MTC with some channel systems	very chaotic sedimentary patterns, probably low reservoir properties	NO							528	
15-A	1400	275	Plastered Drift D1		NO						275		
15-B	1360	270	Submarine channel covered by a contouritic terrace (T2)		NO			135		135			
15-C	1456	283	Submarine channel covered by a contouritic terrace (T2)		NO			142		142			

Acumulation	Water depth (m)	BSR depth (mbsf)	Geological interpretation	Comments	Interval of interest identified	Average thickness of interest interval (m)	Thickness in m of the interpreted deposit types within the interval of interest or GHSZ						Expected reservoir quality
							Turbidite	Channel fill	Shelf to Slope Progradations	Contouritic Terrace	Contouritic Drift	Mass Transport	
16	2311	491	MTC		NO							491	
17	3289	540	MTC		NO							540	
18-A	**1409**	**291**	Possibly contourite drift over a MTC	Blanking above BSR and marked high amplitudes below BSR suggest presence of hydrates	**YES**	**58**					**58**		**Low**
19	1503	284	Mass transport deposits and contourite drift (D1)		NO						95	189	
20	854	189	Smooth upper slope progradation and channel system below		NO				189				
21	1008	204	Smooth upper slope progradation and contouritic terrace T1 with channel system below		NO			102			102		
22-A	**1449**	**356**	Eroded plastered drift D1 on top of a complex channel system.	There is blanking on one body suggesting the presence of hydrates.	**YES**	**51**		**51**					**Medium-High**
22-B	1388	313	Plastered Drift D1 on top of a complex channel system	blanking suggesting the presence of hydrates.	NO			209			104		

Acumulation	Water depth (m)	BSR depth (mbsf)	Geological interpretation	Comments	Interval of interest identified	Average thickness of interest interval (m)	Thickness in m of the interpreted deposit types within the interval of interest or GHSZ						Expected reservoir quality
							Turbidite	Channel fill	Shelf to Slope Progradations	Contouritic Terrace	Contouritic Drift	Mass Transport	
23	2595	471	Eroded plastered drift D1 and Concave erosive Lower slope with Mass Transport Deposits		NO						236	236	
24	3126	525	Mass transport deposits		NO							525	
25	**872**	**243**	Possibly turbiditic deposits , deposited over a mass transport deposit and overlayed by smooth upper slope progradation		**YES**	**41**	**41**						**High**
26	1072	273	Contouritic terrace T2 (Ewing terrace) and MTC	No distinct body detected	NO					91		182	
27	696	98	start of submarine canyon system on top and MTC (debris flow?) below.	Close to the limit of the BSR towards the seafloor. No distinct body detected	NO				98				
28	658	132	Smooth upper slope progradation	Close to the limit of the BSR towards the seafloor. No distinct body detected	NO				132				
29	1023	275	Steep progradational middle slope with some canyons systems and MTC below	No distinct body detected	NO			92	92			92	

Acumulation	Water depth (m)	BSR depth (mbsf)	Geological interpretation	Comments	Interval of interest identified	Average thickness of interest interval (m)	Thickness in m of the interpreted deposit types within the interval of interest or GHSZ						Expected reservoir quality
							Turbidite	Channel fill	Shelf to Slope Progradations	Contouritic Terrace	Contouritic Drift	Mass Transport	
30	1941	371	Steep progradational middle slope towards the north with some canyons systems. Eroded pastered drift D1 and and MTC toward the south	No distinct body detected	NO						74	297	
31	2408	470	convex undisturbed seafloor with MTC	No distinct body detected	NO							470	
32-A	**2210**	**456**	plastered drift D1 on top, contourites and Mass transport deposits	Not close to the BSR (low hidrate saturation?)	**YES**	**38**					**38**		**Low**
33	910	259	steep progradational middle slope	No distinct body detected	NO						259		
34-A	**1285**	**323**	steep progradational middle slope. Channel fill body in between mass transport deposits	Blanking observed where the body is closer to the BSR	**YES**	**43**		**43**					**Medium-High**
35-A	**765**	**189**	Steep progradational middle slope. Close to the limit between BSR and seafloor	Body presenting strong blanking (buried drift?)	**YES**	**51**					**51**		**Low**
36	1256	249	Plastered drifts over terrace T2	No distinct body detected	NO						249		

Acumulation	Water depth (m)	BSR depth (mbsf)	Geological interpretation	Comments	Interval of interest identified	Average thickness of interest interval (m)	Thickness in m of the interpreted deposit types within the interval of interest or GHSZ						Expected reservoir quality
							Turbidite	Channel fill	Shelf to Slope Progradations	Contouritic Terrace	Contouritic Drift	Mass Transport	
37	1669	307	Plastered drift D1	No distinct body detected	NO						307		
38	1852	302	Plastered drift	No distinct body detected	NO						302		
39	1494	222	Plastered drift	No distinct body detected	NO						302		

Appendix K Sensitivity to Permeability for Prospect HP25

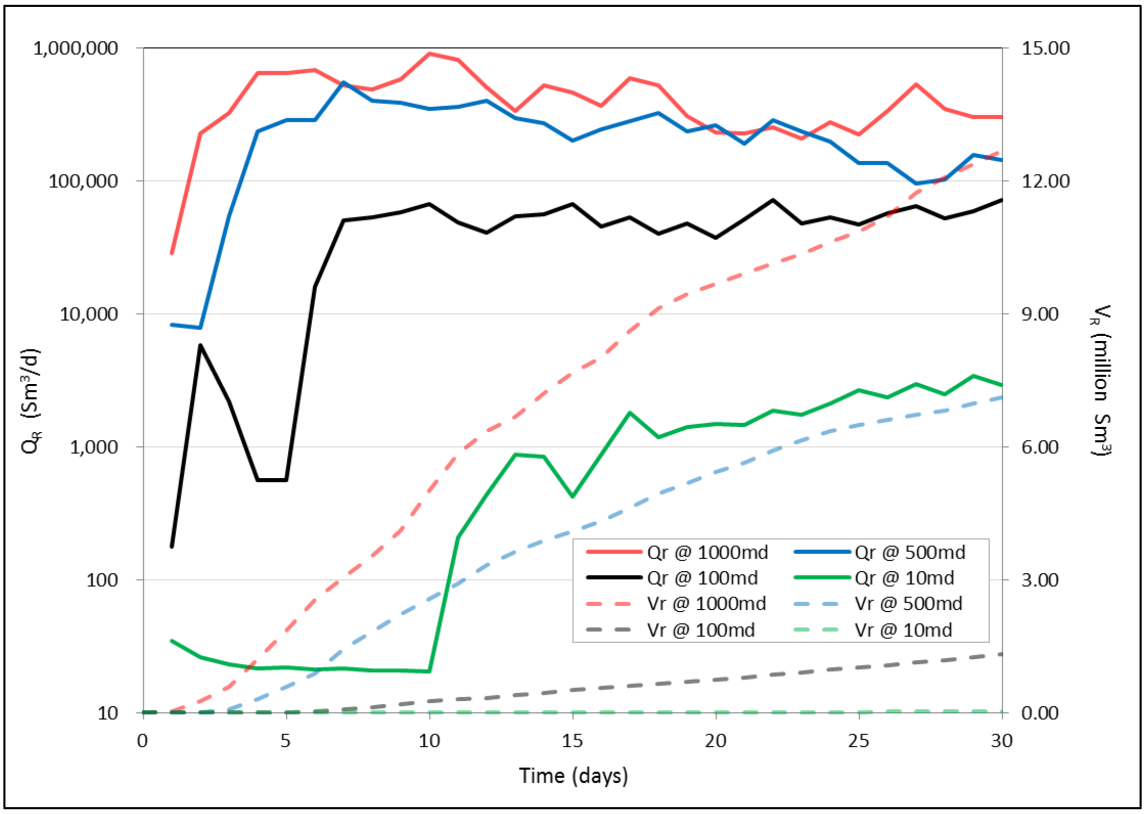

Fig. I-1 Sensitivity analysis to permeability showing gas release rate and cumulative gas volume from prospect HP25

Appendix L Spatial distribution of S_H for both prospects

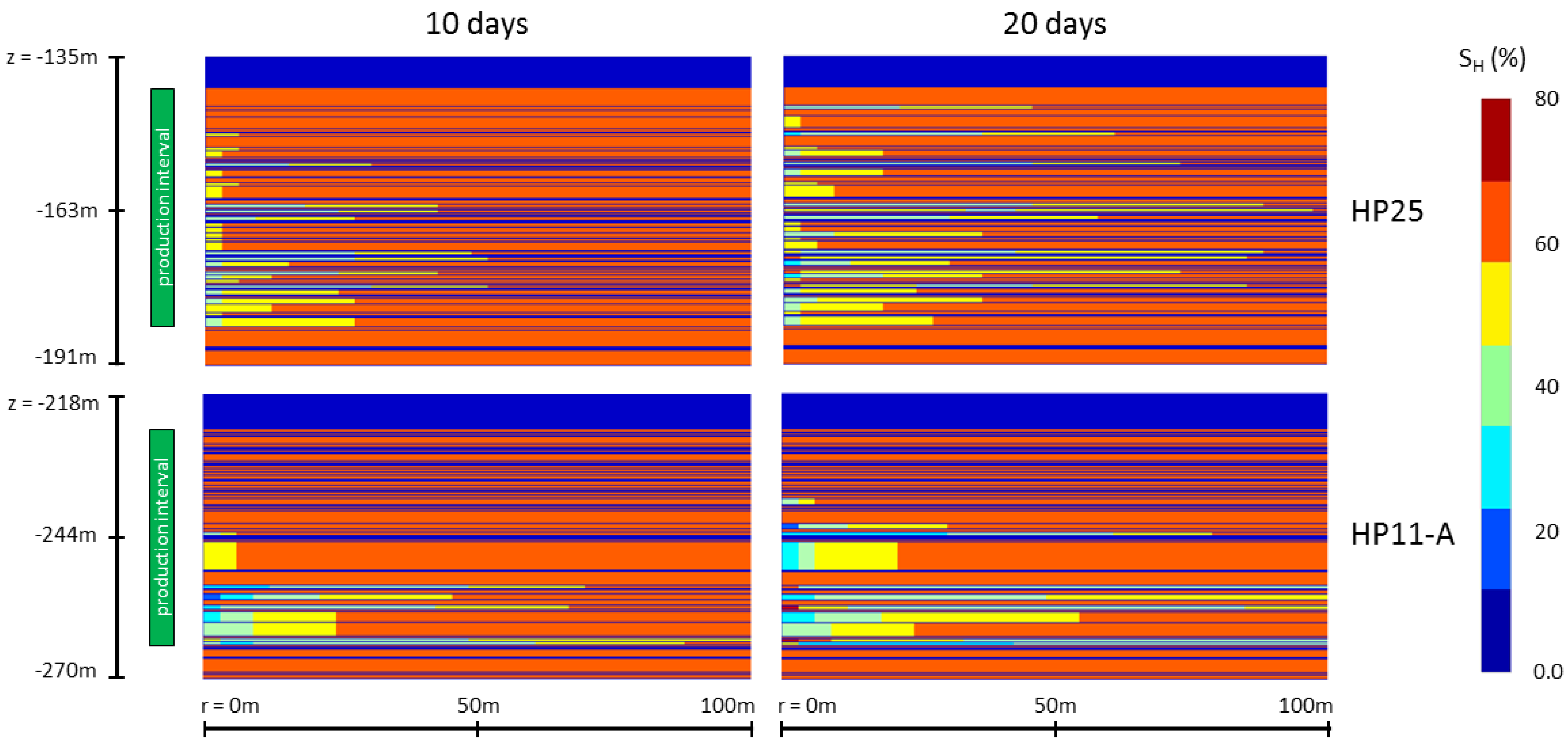

Fig. L-1 Spatial distribution of S_H for both prospects at 10 and 20 days (approximate times at which the hydrate dissociation front reach the model boundary)